Eur. Phys. J. C (2025) 85:277
https://doi.org/10.1140/epjc/s10052-025-14006-2

THE EUROPEAN PHYSICAL JOURNAL C

Regular Article - Theoretical Physics

Deciphering $\Lambda(1405)$ state via mass, compositeness and magnetic moment

Halil Mutuk[a]

Department of Physics, Faculty of Sciences, Ondokuz Mayis University, 55200 Samsun, Turkey

Received: 9 December 2024 / Accepted: 24 February 2025

Abstract The $\Lambda(1405)$ state has strangeness $S = -1$ and isospin $I = 0$ with quantum number $J^P = 1/2^-$. It is located just below the threshold of $\bar{K}N$. In this study, the internal structure of the $\Lambda(1405)$ state is investigated based on meson-baryon molecular configuration using one-boson-exchange (OBE) model. We take into account various states (K^-p, K^0n, $K^-p - K^0n$, $\pi^+\Sigma^-$, $\pi^-\Sigma^+$, $\pi^0\Sigma^0$, $\pi^+\Sigma^- - \pi^-\Sigma^+$, $\pi^+\Sigma^- - \pi^0\Sigma^0$ and $\pi^-\Sigma^+ - \pi^0\Sigma^0$ and $\eta\Lambda$) and calculate spectroscopic parameters such as mass and magnetic moment. Some of the predicted masses for the states in this work are below corresponding threshold. The predicted masses of K^-p, K^0n, and $K^-p - K^0n$ states are below $\bar{K}N$ threshold whereas predicted masses of $\pi^+\Sigma^-, \pi^-\Sigma^+, \pi^0\Sigma^0, \pi^+\Sigma^- - \pi^-\Sigma^+, \pi^+\Sigma^- - \pi^0\Sigma^0$, and $\pi^-\Sigma^+ - \pi^0\Sigma^0$ states are below $\pi\Sigma$ threshold. These states may be bound state candidates. We obtain that all the states of this present work have sizes larger than the confinement scale, ($1/\Lambda_{\rm QCD} \sim 1$ fm). We also study compositeness criterion for these states. Using compositeness criterion, we calculate scattering length a_s and effective range r_e. The results reflect that the present states of this work have compositeness dominance, i.e., they are in molecular configuration. The magnetic moment results yield that the magnetic moment is mainly dominated by the corresponding baryon component. Our results of magnetic moments support $\bar{K}N$ molecular configuration for $\Lambda(1405)$.

1 Prolog

The $\Lambda(1405)$ state remains to be an interesting case despite the fact that more than 50 years passed through its observation. Theoretically the prediction of the $\Lambda(1405)$ was done in the year 1959 [1] and experimental observation was announced in 1961 [2,3]. The quark model predicted this state to be a conventional baryon composed of uds quark flavours, to be more exact, first orbitally excited state of uds. Nonetheless, $\Lambda(1405)$ does not fit to conventional quark model properly. Having a strange quark content should make this state heavier than its non-strange counterparts, for example $N(1535)$, but the lower mass than its non-strange counterparts takes out this state from the framework of quark model. The other evidence which makes this state intriguing is that, assuming $\Lambda(1520)$ as the spin-orbit partner of $\Lambda(1405)$, the mass difference between spin-orbit partners is significantly larger compared to nucleon sector, for example $N(1535)$ and $N(1520)$.

The Particle Data Group (PDG) [4] gives average mass and width values of $\Lambda(1405)$ state as

$$M = 1405.1^{+1.3}_{-0.9}\ \text{MeV},\ \ \Gamma = 50.5 \pm 2.0\ \text{MeV}, \tag{1}$$

respectively. This state is annotated as a four-star state in PDG. After the observation of $\Lambda(1405)$, it was first investigated in quark model as an ordinary baryon. Refs. [5,6] obtained the mass around 1.6 GeV. Lattice QCD study on this state yielded a mass about 1.7 GeV which is much heavier than the actual mass [7]. Clearly, it can be seen that conventional quark model fails to predict the mass of $\Lambda(1405)$. This discrepancy paved the way for other possible structures. Since the mass of $\Lambda(1405)$ is close to the $\bar{K}N$ threshold, it was conjectured in Ref. [1] to be a molecular-type bound state before the introduction of the quark model. In Refs. [8,9], chiral unitary approach was applied to $\Lambda(1405)$ state examining the behavior of number of colors (N_c). These studies observed that SU(3) singlet $\bar{K}N$ component of the $\Lambda(1405)$ state survives in the large (N_c) limit. S-wave meson-nucleon interaction is adopted in the coupled-channel Lippmann–Schwinger equations for $S = -1$ sector in which $\Lambda(1405)$ resonance was reproduced successfully [10]. In Ref. [11], $I = 0$ $\bar{K}N$ interaction was investigated supporting a $\bar{K}N$

[a] e-mail: hmutuk@omu.edu.tr (corresponding author)

Published online: 12 March 2025

bound state. The calculation in the MIT Bag model [12] gave a mass of 1400 MeV for a $\Lambda(1405)$ state in the five-quark state. Dynamical coupled-channel approach was used in Ref. [13]. They obtained a dominant meson-baryon component in the $\Lambda(1405)$ structure. The meson-baryon structure was also investigated by using the chiral unitarity approach [13]. A dominant meson-baryon molecule component was also found for the $\Lambda(1405)$ structure. Ref. [14] used the same approach in order to obtain electromagnetic mean squared radii of the $\Lambda(1405)$ state giving a larger size compared to the ground state of conventional baryons. In Ref. [15], $\bar{K}N$ state was considered as a K^-p bound state in a variational treatment revealing a molecular feature. The five-body problem as $q^4\bar{q}$ system and traditional baryon solved for $\Lambda(1405)$ in a realistic quark model with a confinement potential, one gluon exchange potential, and π, K and σ exchange potentials [16]. They observed that the energy of $q^4\bar{q}$ state as $\Lambda(1405)$ was lower than that of traditional baryon state. In Ref. [17], constituent quark model with SU(3) flavor symmetry was applied to $\Lambda(1405)$ which resulted $\Lambda(1405)$ to be a mixture of the P-wave q^2s state and ground $q^3s\bar{q}$ state. Using Jaffe and Wilczek's diquark model, three negative parity Λ particles were predicted within the range between 1400 and 1540 MeV [18]. The existence of $\Lambda(1405)$ with $J^P = \frac{1}{2}^-$ as a pentaquark state was discussed. Refs. [19,20] considered $\Lambda(1405)$ as a quasi-bound state of $\bar{K}N$. The root mean square radius of $\bar{K}N$ was obtained as 1.3 fm [19]. The studies mentioned here have a single pole dominance.

In the past 20 years, experiments revealed some indications of distortion from a single pole [21,22]. Prior to these experimental findings, two-pole structure was identified in Ref. [23]. Using the data from CLAS collaboration [22], chiral unitary approach was applied to two-pole structure of $\Lambda(1405)$ which gave clues about existence of two poles [24,25]. According to recent experimental data provided by BGOOD collaboration [26], ALICE collaboration [27], and GlueX collaboration [28], two-pole structure was supported. However, a comprehensive analysis [29] of the data provided by CLAS Collaboration and recent data from J-PARC experiment [30] indicated that a single resonance is sufficient to describe the data, on the other hand, the possibility of two-pole structure is not ruled out definitely. For example, a very recent constituent quark model study of $\bar{K}N$ finds two poles in the isoscalar $J^P = \frac{1}{2}^-$ sector for the $\Lambda(1405)$ state [31]. While some studies suggest two-pole structure for $\Lambda(1405)$, the properties and location of the second resonance remain unclear. See the recent studies [32–35] and references therein for further discussion.

Despite the fact that numerable studies with various models [31,36–79] are conducted for the properties of $\Lambda(1405)$ state, there is no agreement on the structure of the $\Lambda(1405)$ state and its nature remains still unclear. The aforementioned studies adopt different possibilities such as a compact four-quark state, a hybrid baryon, or a meson-baryon molecule. The latter one seems to be a possible scenario based on the data for invariant mass spectra of $\pi^{\pm}\Sigma^{\mp}$, $\pi^0\Sigma^0$, and $\pi^-\Sigma^0$ [30].

Quantum chromodynamics (QCD) is the accepted theory of the strong force. It is well known that hadronization occurs at lower energies. The breakdown of perturbation theory in QCD at low energies makes this an important phenomenon for our understanding of QCD. In this respect, the exotic states and candidates are important probes for improving our realization of the QCD at low energy. The calculation of mass is an important ingredient in hadron spectroscopy. It may help to classify the particles. In addition to this, electromagnetic properties are useful probes to determine the internal configurations of the hadrons. They give valuable information about the shape of the hadrons, charge distribution and response to magnetic field. The obtained magnetic moment value may be employed to delineate the distribution of quark-antiquark pairs inside the hadron using OBE interaction potential.

Most of the multiquark hadrons are expected to be in molecular configuration. Molecular states composed of a hadron pair seem to be a favorite explanation since the observations often take place near the threshold of a corresponding pair of hadrons. In this context, we study masses, compositeness criterion, and magnetic moments of $\Lambda(1405)$ as meson-baryon molecules of $\bar{K}N$, $\pi\Sigma$ and $\eta\Lambda$ states using OBE model.

In the next section, we provide the details of the model of this work. In Sect. 2, we present the model of this work. Additionally, we introduce the potential model, compositeness criterion and magnetic moment in related subsections. Section 3 is dedicated to a comprehensive analysis of the mass spectra, compositeness criterion, and magnetic moments. Finally this work ends with the summary in Sect. 4.

2 Formalism

2.1 Theoretical framework

Understanding the interaction between nucleons have a long history in high energy physics. The oldest theory of nuclear forces was proposed by Yukawa [80]. In 1935, the proposal of Yukawa which explains the strong nuclear force generated through the exchange of particles with finite mass, led to the discovery of the pion. The Yukawa's idea was the first building block of the so-called one-pion exchange theory. Following the theory of Yukawa, one-pion and two-pion exchange potentials were applied to nucleon-nucleon (NN) scattering data in the first years of 1950 [81,82]. Later, it was found that exchange of vector bosons was needed to explain experimental data. It was realized that ρ and ω contribute spin-orbit

interaction and repulsive core at short internucleon distances based on the (NN) scattering [83]. These elaborations led to the birth of OBE model.

In the OBE model, the interaction between the hadrons is generated via exchanging mesons composed of up (u) and down (d) quarks. Strange quarks (s) may also contribute the interaction when the corresponding hadron consists s quark [84–88]. The successful applications of OBE potential models stem from the following realms [89]: (i) OBE potential models provide insightful physical mechanism for the interaction between nucleons. The parameters in OBE potential models have physical meanings, and can be related to or may be determined through other physical processes. The physical meson parameters are common to the entire interaction. (ii) Constructing consistent electroweak currents for systems interacting via OBE is possible. Ref. [90] obtained exchange currents that are needed for current conservation for (NN) interaction in which microscopic processes are known. (iii) Using OBE in a covariant formalism excluding time ordering, three-body and many-body forces are spontaneously produced from the off-shell couplings of purely two-body OBE model [91,92]. In phenomenological potentials, three-body forces need to be independently constructed and adjusted to the model. (iv) The OBE model is based on a limited number of parameters and provides an accurate representation of the (NN) interaction.

OBE model has been an invaluable and useful tool in describing hadron-hadron interactions. However, OBE models have their restrictions. Interactions of OBE model are not fundamental interactions, so that their validity may not extend to very short distances where due to asymptotic freedom, QCD should have correct description. This is acceptable because in extremely short distances, the OBE potential is not expected to work. In phenomenological potentials, the short-range behavior of the interaction is generally parametrized phenomenologically through vertex form factors with proper parameters.

The study of meson-baryon molecules has garnered significant interest in recent years due to the discovery of various exotic hadronic states. These states, which include both meson-meson and meson-baryon interactions, provide a rich field for exploring the dynamics of strong interactions and the underlying principles of QCD. Hadronic molecules have emerged as a significant area of interest in hadron spectroscopy, particularly following numerous experimental discoveries in the heavy quarkonium sector that defied the predictions of the traditional quark model. These discoveries have revitalized the study of hadron structures, leading to a deeper exploration of hadronic molecules, which are analogous to light nuclei and can be predicted with controlled uncertainty.

Hadronic molecules can be regarded as analogs of light nuclei, most notably the deuteron. The deuteron is a shallowly bound state of the proton and neutron, and located just below the neutron-proton continuum threshold. Furthermore, it is an extended object which has a size of ≈ 2.12 fm. These two features, having a mass just below the corresponding threshold and a sizeable spatial extension, can be used to define hadronic molecules, see Ref. [93] for details of hadronic molecules.

In this paper, we adopt an OBE potential model for studying meson-baryon molecular states. This potential model is called Bonn potential model [94]. The Bonn potential, which is a sophisticated (NN) interaction model, has been instrumental in advancing our understanding of nuclear forces. Developed through the framework of OBE models, the Bonn potential incorporates the exchange of various mesons to describe the interaction between nucleons. This model has undergone several refinements to enhance its precision and applicability in different nuclear physics contexts. This model has been also extended to describe meson-baryon interactions, predicting strongly attractive S-wave interactions in both isospin 0 and 1 states [95].

The Hamiltonian of meson-baryon molecule reads as

$$H = \sqrt{P^2 + m_{h_1}^2} + \sqrt{P^2 + m_{h_2}^2} + V_{hh}, \tag{2}$$

where m_{h_1} and m_{h_2} are the masses of constituents, P is the relative momentum of two hadrons, and V_{hh} is the inter-hadronic interaction potential. The dihadronic interaction potential is given by

$$V_{hh} = V_{\text{OBE}} + V_Y, \tag{3}$$

where V_{OBE} is the OBE potential and V_Y is screened Yukawa-like potential. One of the key strengths of the OBE potential model is its ability to incorporate different types of mesons, including pseudoscalar, vector, and scalar mesons, each contributing uniquely to the potential. Meson exchange models play a crucial role in understanding the (NN) interaction, which is fundamental to nuclear physics. These models describe the forces between nucleons in terms of meson exchanges, providing insights into the underlying mechanisms of nuclear forces. The OBE potential is the sum of the one-meson-exchange terms

$$V_{\text{OBE}} = V_{ps} + V_s + V_v. \tag{4}$$

In the above equation, V_{ps} denotes the interaction potential for the pseudoscalar meson (π, η), V_s denotes the interaction potential for the scalar meson (σ, a_0), and V_v denotes the interaction potential for vector meson (ω, ρ). The explicit expressions for the interaction potentials are as follow [94]:

$$V_{ps} = \frac{1}{12}\left[\frac{g_{\pi qq}^2}{4\pi}\left(\frac{m_\pi}{m}\right)^2 \frac{e^{-m_\pi r_{ij}}}{r_{ij}} (\tau_i \cdot \tau_j) + \frac{g_{\eta qq}^2}{4\pi}\left(\frac{m_\eta}{m}\right)^2 \frac{e^{-m_\eta r_{ij}}}{r_{ij}}\right](\sigma_i \cdot \sigma_j), \quad (5)$$

$$V_s = -\frac{g_{\sigma qq}^2}{4\pi} m_\sigma \left[1 - \frac{1}{4}\left(\frac{m_\sigma}{m}\right)^2\right] \frac{e^{-m_\sigma r_{ij}}}{m_\sigma r_{ij}} + \frac{g_{\delta qq}^2}{4\pi} m_\delta \left[1 - \frac{1}{4}\left(\frac{m_\delta}{m}\right)^2\right] \frac{e^{-m_\delta r_{ij}}}{m_\delta r_{ij}} (\tau_i \cdot \tau_j), \quad (6)$$

$$V_v = \frac{g_{\omega qq}^2}{4\pi}\left(\frac{e^{-m_\omega r_{ij}}}{r_{ij}}\right) + \frac{1}{6}\frac{g_{\rho qq}^2}{4\pi}\frac{1}{m^2}(\tau_i \cdot \tau_j)(\sigma_i \cdot \sigma_j)\left(\frac{e^{-m_\rho r_{ij}}}{r_{ij}}\right). \quad (7)$$

Finite size effects on the OBE potential with respect to extended structure of the hadrons can be written as

$$V_\alpha\left(r_{h_1h_2}\right) = V_\alpha\left(m_\alpha, r_{h_1h_2}\right) - F_{\alpha 2} V_\alpha\left(\Lambda_{\alpha 1}, r_{h_1h_2}\right) + F_{\alpha 1} V_\alpha\left(\Lambda_{\alpha 2}, r_{h_1h_2}\right), \quad (8)$$

where $\alpha = \pi, \eta, \sigma, \delta, \omega$ and ρ mesons, and

$$\Lambda_{\alpha 1} = \Lambda_\alpha + \epsilon,\ \Lambda_{\alpha 2} = \Lambda_\alpha - \epsilon,$$
$$F_{\alpha 1} = \frac{\Lambda_{\alpha 1}^2 - m_\alpha^2}{\Lambda_{\alpha 2}^2 - \Lambda_{\alpha 1}^2},\ F_{\alpha 2} = \frac{\Lambda_{\alpha 2}^2 - m_\alpha^2}{\Lambda_{\alpha 2}^2 - \Lambda_{\alpha 1}^2}. \quad (9)$$

Here, the subscript α denotes mesons ($\pi, \eta, \sigma, \delta, \omega$ and ρ)$\epsilon/\Lambda_\alpha \ll 1$, thus $\epsilon = 10$ MeV is an appropriate choice.

The use of the form factor

$$F_\alpha(q^2, \Lambda_\alpha) = \left(\frac{\Lambda_\alpha^2 - m_\alpha^2}{\Lambda_\alpha^2 + q^2}\right)^n, \quad (10)$$

at each vertex in the related Feynman diagrams leads to Eq. (8). These diagrams are related to meson exchange contributions. The $V_\alpha(m_\alpha, r)$ term is the related potential for the related mesons (pseudoscalar, scalar, vector). This relation provides an expression that arises in the context of meson exchange potentials. Specifically, it includes the interaction terms for vector mesons, scalar mesons, and pseudoscalar mesons. The equation describes the contributions of these mesons to the nucleon-nucleon interaction through terms that depend on meson properties such as masses, couplings, and spatial configurations.

Screened Yukawa-like potential reads as

$$V_Y = -\frac{k_{mol}}{r_{ij}} e^{\frac{-c^2 r_{ij}^2}{2}}, \quad (11)$$

where k_{mol} is the residual running coupling constant and c represents screen fitting parameter. The screened Yukawa-like potential is used to account for medium-range interactions and incorporates a screening factor to capture effects beyond the typical range of the OBE potential. The screened Yukawa-like potential complements the OBE potential by addressing effects that are not explicitly captured by single-meson exchange contributions, such as higher-order correlations or environmental factors. The molecular states are extended objects. The idea that the two color neutral states interact like dipoles-which are caused by an unequal distribution of color charges within the hadrons-is responsible for this extra potential. Therefore screened Yukawa-like potential incorporates the additional attractive part to the OBE potential to form bound states.

The residual running coupling constant can be determined by

$$k_{mol}\left(M^2\right) = \frac{4\pi}{\left(11 - \frac{2}{3}n_f\right)\ln\frac{M^2 + M_B^2}{\Lambda_Q^2}}, \quad (12)$$

where $M = 2m_{h_1}m_{h_2}/\left(m_{h_1} + m_{h_2}\right)$, m_{h_1} and m_{h_2} are constituent hadron masses of dihadronic system, $M_B = 1$ GeV, Λ_Q is the QCD scale parameter and taken 0.413 and 0.250 GeV for light and heavy mesons, respectively. n_f is the number of flavour [96,97].

The masses of hadrons and exchange mesons are taken from PDG [4]. The coupling constants of the exchange mesons and regularization parameters Λ_α are same as used in Refs. [94,95]. The parameters are listed in Table 1.

Cutoff parameters in the OBE model regulate the meson-nucleon vertices, accounting for the extended structure of hadrons and ensuring a finite interaction range. These cutoffs serve several critical functions: (i) phenomenological regularization in which cutoffs prevent unphysical divergences in the integrals over high-momentum transfers in scattering and bound-state equations. Cutoffs suppress short-range contributions (high-momentum transfers) that are poorly constrained by experimental data or are physically irrelevant

Table 1 Parameters of Bonn potential

Mesons	π	η	σ	a_0	ω	ρ
$\frac{g_{\alpha NN}^2}{4\pi}$	13.6	3	7.7823	2.6713	20	0.85
Λ_α	1.3	1.5	2.0	2.0	1.5	1.3
Mass (in MeV)	134.9	548.8	710	983	782.6	775.4

in low-energy NN interactions. (ii) finite size of hadron: although all phenomenological models assume the constituents as point-like particles, the baryons and mesons are not point particles; cutoff parameters mimic the suppression of high-momentum components due to their finite size. They approximate the finite size of nucleons and mesons, matching observed scattering phase shifts and bound state properties. (iii) connection to experimental data: cutoffs help fit observed NN scattering data and reproduce experimental phase shifts and effective ranges.

Cutoffs are typically parameterized through form factors, (c.f. Eq. (10)). The choice of Λ_α has a direct impact on the strength and range of the interaction. Coupling constants are derived from are derived from experimental data, such as NN scattering cross sections, or are chosen to fit phase shift analyses. Cutoffs reflect the non-pointike structure of mesons and nucleons and significantly influence the off-shell behavior of the potential.

The coupling constants of OBE potential are estimated in the realistic potentials [94,95,98] which were used to reproduce (NN) phase shift data and to study properties of deuteron. Based on the conlusions of regarding references, we assume that

$$g_{\alpha NN} \simeq g_{\alpha hh}, \tag{13}$$

where $g_{\alpha NN}$ is the meson-nucleon coupling constant and $g_{\alpha hh}$ is the meson-hadron coupling constant. By solving Schrödinger equation numerically, we obtain mass spectrum of the $\bar{K}N$, $\pi\Sigma$, and $\eta\lambda$ states.

The observed scaling trend of the effective coupling constant of meson exchange may alter the strength of the interaction potential. It is evident that the precise determination of the intensity of the individual meson exchange potential in the hadron-meson-hadron interaction is contingent upon the knowledge of the effective strength of the coupling constant. It should be noted that the light exchange meson process is unique to each hadron and can be inferred from experimental data or from symmetry principles. Determining the quantum numbers for which the interaction potential results in a molecular bound state is the aim of the current investigation. Therefore, to determine the model parameters, we have approximated the meson-hadron coupling constant.

2.2 Compositeness criterion

The Weinberg compositeness criterion has been a pivotal tool in understanding the nature of hadronic states, particularly in distinguishing between genuine quark states and those dynamically generated by meson-baryon interactions. This criterion, originally formulated for bound states, has been extended to resonant states and higher partial waves, providing deeper insights into the structure of various baryonic resonances.

The usage of scattering length and effective range theory in describing low-energy properties of a two-body system in high energy and nuclear physics is a well established phenomena. One of the sophisticated way to identify whether a particle is composite or not is to apply Weinberg compositeness criterion. In 1965, Weinberg suggested an elegant method to investigate the possibility of deuteron to be an elementary particle, rather than a composite bound state of proton and neutron [99,100]. This analysis connect the field renormalization constant Z (the probability of finding particle in a bare elementary state) with effective range expansion parameters, scattering length a_s and effective range r_e,

$$\begin{aligned} a_s &= [2(1-Z)/(2-Z)]\, R + \mathcal{O}(R_{\rm typ}), \\ r_e &= [-Z/(1-Z)]\, R + \mathcal{O}(R_{\rm typ}), \end{aligned} \tag{14}$$

where $R \equiv 1/\gamma, \gamma = \sqrt{2\mu E_B}$, E_B is the binding energy, μ is the reduced mass of the composite system, and $\mathcal{O}(R_{\rm typ})$ is the typical length scale of the interaction. Weinberg conjectured that depending on the value of field renormalization constant Z which falls in the range $0 \le Z \le 1$, it can be determined that the state becomes a pure elementary or a pure composite state: for $Z = 0$ then the particle is in a pure composite state, while for $Z = 1$ it becomes a purely elementary.

The application of Weinberg criterion to deuteron can be done in the following way. Firstly, letting $Z = 0$ which means deuteron is a composite particle, Eq. (14) becomes $a_s = R$ and $r_e = \mathcal{O}(R_{\rm typ})$. This is just a theoretical assertion and should be confronted with the experimental data, if available. The scattering length a_s and effective range r_e are extracted from the experimental data. Using proton-neutron scattering data in the deuteron channel [101], the scattering length a_s and effective range r_e can be obtained as

$$a_s = -5.41 \text{ fm}, r_e = 1.79 \text{ fm}. \tag{15}$$

The deuteron binding energy reads [102]

$$E_B = 2.22 \text{ MeV} \to \gamma = 45.7 \text{ MeV} = 0.23 \text{ fm}^{-1}. \tag{16}$$

The range of forces in the deuteron is provided by the pion mass and can be estimated

$$R_{\rm typ} \simeq \frac{1}{M_\pi} \simeq 1.4 \text{ fm}. \tag{17}$$

This result agrees with the experimental data and reflects that the effective range is positive and of the order of the range corrections as required by the compositeness criterion. Taking $Z = 0$, scattering length yields [93]

$$a_s = -(4.3 \pm 1.4) \text{ fm} \tag{18}$$

which is consistent for experimental data. The minus sign is just the convention used in the related reference. In contrast, if the deuteron is a pure elementary state or has a significant probability Z (> 0.2) of being in an elementary state, then scattering length a_s should be less than R, and effective range r_e would be large and negative. This is clearly a contradiction with the experimental data. Therefore, based on these considerations it can be said that deuteron is composite particle.

2.3 Magnetic moment

The study of magnetic moments in hadrons provides critical insights into the internal structure and dynamics of these particles, governed by the principles of QCD. Magnetic moments are fundamental properties that reveal the distribution of charge and magnetization within hadrons. They are particularly useful for understanding the geometrical shapes and quark-gluon organization of these particles. This endeavour is essential for understanding the geometrical shapes and quark-gluon organization within hadrons, which can further aid in the identification and characterization of various hadronic states. In the context of meson-baryon molecules, understanding magnetic moments can shed light on the dynamics and binding mechanisms within these systems.

The study of meson-baryon molecules has garnered significant interest in recent years due to the discovery of various exotic hadronic states. These states, often interpreted as molecular-like structures, provide a unique window into the strong interaction dynamics that govern the behavior of quarks and gluons. The concept of meson-baryon molecules extends the traditional quark model by considering the binding of mesons and baryons through mechanisms such as isospin-exchange attraction and one-boson exchange potentials.

The Bonn model does not incorporate quark masses. Therefore, for calculating magnetic moments we rely on constituent quark model. At the quark level, the magnetic moment operators can be written as

$$\hat{\mu} = \sum_i \frac{q_i}{2m_i}\hat{\sigma}_i, \tag{19}$$

where q_i is the quark charge, m_i is the quark mass, and $\hat{\sigma}_i$ is the Pauli spin matrix of the i-th quark, respectively. Due to hadronic molecule picture considered in this work, it will be useful to calculate magnetic moments in this picture. In Fig. 1, meson-baryon molecule configuration is schematized.

Since the constituents of the molecular states are separated from each other relatively away in molecular configuration, the magnetic moment of the molecular pentaquark state is closely related to the magnetic moment of the meson and

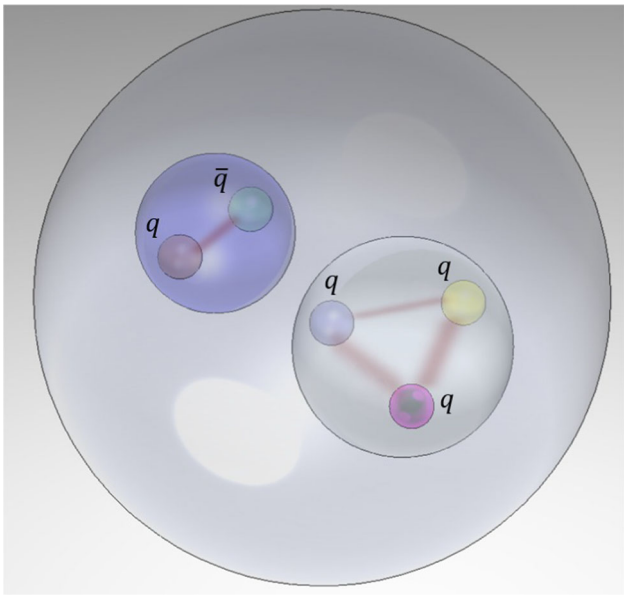

Fig. 1 Schematic diagram of meson-baryon molecule

magnetic moment of the baryon. Therefore, the magnetic moment of the S-wave meson-baryon molecule consists of the sum of the meson magnetic moment and the baryon magnetic moment [103–105]

$$\hat{\mu} = \hat{\mu}_M + \hat{\mu}_B, \tag{20}$$

where the subscripts M and B represent meson and baryon, respectively. The magnetic moment can be extracted via calculating

$$\mu = \langle \Psi_M | \hat{\mu}_M | \Psi_M \rangle + \langle \Psi_B | \hat{\mu}_B | \Psi_B \rangle \tag{21}$$

where Ψ_M and Ψ_B denote the total wave function of the meson and baryon, respectively. The total wave function can be decomposed into

$$\Psi = \phi_{flavor} \otimes \chi_{spin} \otimes \xi_{color} \otimes \eta_{space}. \tag{22}$$

As a result of Fermi statistics, the total wave function should be antisymmetric. In the meson-baryon molecular picture, the relationship between spin and flavor is $(\phi_{flavor} \otimes \chi_{spin})$ is symmetric. This is due to the fact that color wave function is antisymmetric and the spatial wave function is symmetric in the ground state. The magnetic moment calculation requires taking into account the symmetry requirement of the flavor-spin wave function. The wave functions for mesons and baryons are tabulated in Tables 2 and 3, respectively.

Obtaining magnetic moment is a straightforward calculation which includes the expectation value of the flavor wave function and spin wave function of the related hadron. As an example, we derive the magnetic moment formula of MB

Table 2 The flavor wave functions ϕ_{flavor} and the spin wave functions χ_{spin} of the S-wave mesons

Meson	$\phi_{flavor} \otimes \chi_{spin}$
π^+	$u\bar{d} \otimes \frac{1}{\sqrt{2}}(\uparrow\downarrow - \downarrow\uparrow)$
π^0	$\frac{1}{\sqrt{2}}(u\bar{u} - d\bar{d}) \otimes \frac{1}{\sqrt{2}}(\uparrow\downarrow - \downarrow\uparrow)$
π^-	$d\bar{u} \otimes \frac{1}{\sqrt{2}}(\uparrow\downarrow - \downarrow\uparrow)$
η	$\frac{1}{\sqrt{6}}(u\bar{u} + d\bar{d} - 2s\bar{s}) \otimes \frac{1}{\sqrt{2}}(\uparrow\downarrow - \downarrow\uparrow)$
K^0	$d\bar{s} \otimes \frac{1}{\sqrt{2}}(\uparrow\downarrow - \downarrow\uparrow)$
K^-	$s\bar{u} \otimes \frac{1}{\sqrt{2}}(\uparrow\downarrow - \downarrow\uparrow)$

(meson-baryon) state. Let M meson has $S = 1$ and spin and flavor wave function be

$$\phi_{meson} = |q_1\bar{q}_2\rangle, \quad \chi_{meson} = |\uparrow\uparrow\rangle. \tag{23}$$

Let the B baryon has $S = 3/2$ and spin and flavor wave function be

$$\phi_{baryon} = |q_3q_4q_5\rangle, \quad \chi_{baryon} = |\uparrow\uparrow\uparrow\rangle. \tag{24}$$

The magnetic moment of the molecular MB state can be decomposed as

$$\begin{aligned}\mu &= \langle\phi_{meson} \otimes \chi_{meson}|\hat{\mu}_{meson}|\phi_{meson} \otimes \chi_{meson}\rangle \\ &\quad + \langle\phi_{baryon} \otimes \chi_{baryon}|\hat{\mu}_{baryon}|\phi_{baryon} \otimes \chi_{baryon}\rangle \\ &= \frac{q_1}{2m_{q_1}}\langle\sigma_1\rangle + \frac{\bar{q}_2}{2m_{\bar{q}_2}}\langle\sigma_2\rangle + \frac{q_3}{2m_{q_3}}\langle\sigma_3\rangle + \frac{q_4}{2m_{q_4}}\langle\sigma_4\rangle \\ &\quad + \frac{q_5}{2m_{q_5}}\langle\sigma_5\rangle,\end{aligned} \tag{25}$$

where σ_i are the spin projection of the i-th quark. For this case, the total magnetic moment of the state under consideration turns out to be

$$\mu = \mu_{q_1} + \mu_{\bar{q}_2} + \mu_{q_3} + \mu_{q_4} + \mu_{q_5}. \tag{26}$$

By substituting constituent masses of the quarks one can obtain magnetic moments of other states using their flavor-spin wave function. For this purpose, we use the following set of constituent quark masses [106]

$$m_u = m_d = 0.336 \text{ GeV}, \ m_s = 0.540 \text{ GeV}. \tag{27}$$

3 Numerical results and discussion

In this section, we present our results in the consecutive subsections as in previous section.

3.1 Mass spectrum of $\bar{K}N$, $\pi\Sigma$, and $\eta\Lambda$ states

We obtain S-wave mass values and binding energies of $I = 0$ K^-p, K^0n, $K^-p - K^0n$, $\pi^+\Sigma^-$, $\pi^-\Sigma^+$, $\pi^0\Sigma^0$, $\pi^+\Sigma^- - \pi^-\Sigma^+$, $\pi^+\Sigma^- - \pi^0\Sigma^0$ and $\pi^-\Sigma^+ - \pi^0\Sigma^0$ and $\eta\Lambda$ states. The results are listed in Table 4. The binding energy is defined by $E_B = M_{Model} - M_{Threshold}$, where $M_{Threshold}$ denotes the mass of related meson-baryon threshold.

As mentioned before, the minimal quark content for $\Lambda(1405)$ is uds. Therefore, in theoretical ground the K^-p, K^0n, $K^-p - K^0n$, $\pi^+\Sigma^-$, $\pi^-\Sigma^+$, $\pi^0\Sigma^0$, $\pi^+\Sigma^- - \pi^-\Sigma^+$, $\pi^+\Sigma^- - \pi^0\Sigma^0$, $\pi^-\Sigma^+ - \pi^0\Sigma^0$, and $\eta\Lambda$ states may have the quark content for $\Lambda(1405)$. The binding energies suggest that, all the meson-baryon systems could be bound states with respect to their thresholds. As can be seen in the Table 4, mass of $\eta\Lambda$ state is approximately 200 MeV above $\Lambda(1405)$ mass. According to our model, this state could not be a candidate for $\Lambda(1405)$. The $\pi\Sigma$ threshold is located approximately 100 MeV below the $\bar{K}N$ threshold. The $\pi\Sigma$ states in this work are deeply bounded with respect to $\bar{K}N$ threshold.

Table 3 The flavor wave functions ϕ_{flavor} and the spin wave functions χ_{spin} of the S-wave baryons

Baryon	$\phi_{flavor} \otimes \chi_{spin}$
p	$\frac{1}{\sqrt{2}}\left\{\frac{1}{\sqrt{2}}(2uud - udu - duu) \otimes \frac{1}{\sqrt{6}}(2\uparrow\uparrow\downarrow - \uparrow\downarrow\uparrow - \downarrow\uparrow\uparrow) + \frac{1}{\sqrt{2}}(udu - duu) \otimes \frac{1}{\sqrt{2}}(\uparrow\downarrow\uparrow - \downarrow\uparrow\uparrow)\right\}$
n	$\frac{1}{\sqrt{2}}\left\{\frac{1}{\sqrt{2}}(-2ddu + dud + udd) \otimes \frac{1}{\sqrt{6}}(2\uparrow\uparrow\downarrow - \uparrow\downarrow\uparrow - \downarrow\uparrow\uparrow) + \frac{1}{\sqrt{2}}(udd + dud) \otimes \frac{1}{\sqrt{2}}(\uparrow\downarrow\uparrow - \downarrow\uparrow\uparrow)\right\}$
Σ^+	$\frac{1}{\sqrt{2}}\left\{\frac{1}{\sqrt{6}}(2uus - usu - suu) \otimes \frac{1}{\sqrt{6}}(2\uparrow\uparrow\downarrow - \uparrow\downarrow\uparrow - \downarrow\uparrow\uparrow) + \frac{1}{\sqrt{2}}(usu - suu) \otimes \frac{1}{\sqrt{2}}(\uparrow\downarrow\uparrow - \downarrow\uparrow\uparrow)\right\}$
Σ^0	$\frac{1}{\sqrt{2}}\left\{\frac{1}{\sqrt{12}}(2uds - usd - dsu + 2dus - sud - sdu) \otimes \frac{1}{\sqrt{6}}(2\uparrow\uparrow\downarrow - \uparrow\downarrow\uparrow - \downarrow\uparrow\uparrow) + \frac{1}{2}(usd + dsu - sdu - sud) \otimes \frac{1}{\sqrt{2}}(\uparrow\downarrow\uparrow - \downarrow\uparrow\uparrow)\right\}$
Σ^-	$\frac{1}{\sqrt{2}}\left\{\frac{1}{\sqrt{6}}(2dds - dsd - sdd) \otimes \frac{1}{\sqrt{6}}(2\uparrow\uparrow\downarrow - \uparrow\downarrow\uparrow - \downarrow\uparrow\uparrow) + \frac{1}{\sqrt{2}}(dsd - sdd) \otimes \frac{1}{\sqrt{2}}(\uparrow\downarrow\uparrow - \downarrow\uparrow\uparrow)\right\}$
Λ	$\frac{1}{\sqrt{2}}\left\{\frac{1}{2}(usd + sud - sdu - dsu) \otimes \frac{1}{\sqrt{6}}(2\uparrow\uparrow\downarrow - \uparrow\downarrow\uparrow - \downarrow\uparrow\uparrow) + \frac{1}{\sqrt{12}}(2dsu - dsu - sud - 2dus - sdu + usd) \otimes \frac{1}{\sqrt{2}}(\uparrow\downarrow\uparrow - \downarrow\uparrow\uparrow)\right\}$

Table 4 Mass spectrum and binding energies of possible S- wave meson-baryon states for $\Lambda(1405)$. The results are in unit of MeV

States	K^-p	K^0n	K^-p-K^0n	$\pi^+\Sigma^-$	$\pi^-\Sigma^+$	$\pi^0\Sigma^0$	$\pi^+\Sigma^--\pi^-\Sigma^+$	$\pi^+\Sigma^--\pi^0\Sigma^0$	$\pi^-\Sigma^+-\pi^0\Sigma^0$	$\eta\Lambda$
Masses	1415.8	1420.6	1418.7	1331.9	1324.0	1322.4	1326.9	1327.3	1327	1646.1
Binding	− 15.9	− 16.6	− 16.3	− 5.1	− 4.9	− 5.2	− 4.1	− 3.7	− 4.0	− 17.4

However, the dynamics in the $\pi\Sigma$ and $\bar{K}N$ channels may be quite different. For the time being, there is no experimental information about the $\pi\Sigma$ threshold quantities. In Fig. 2, the locations of masses of $\bar{K}N$, $\pi\Sigma$, and $\eta\Lambda$ states with respect to $\bar{K}N$ and $\pi\Sigma$ thresholds are shown respectively, where we assume isospin averaged masses, $m_\pi = 138$ MeV, $m_{\bar{K}} = 496$ MeV, $m_N = 939$ MeV, and $m_\Sigma = 1193$ MeV. It is clear that, K^-p, K^0n, and K^-p-K^0n states are located below the corresponding $\bar{K}N$ threshold and $\pi^+\Sigma^-$, $\pi^-\Sigma^+$, $\pi^0\Sigma^0$, $\pi^+\Sigma^--\pi^-\Sigma^+$, $\pi^+\Sigma^--\pi^0\Sigma^0$ and $\pi^-\Sigma^+-\pi^0\Sigma^0$ are located very close to $\pi\Sigma$ threshold. It can be seen from the figure that the phase space between the $\eta\Lambda$ and related $\bar{K}N$ and $\pi\Sigma$ thresholds are very large. Although at the quark level, the quark content of $\eta\Lambda$ could refer to the quark content of $\Lambda(1405)$, calculated mass of $\eta\Lambda$ do not support this hypothesis.

We should note that, although the model of this present work is not capable of investigating the two-pole structure for the $\Lambda(1405)$ state, in the coupled-channel approach, the $\Lambda(1405)$ state is attributed as a composotion of two resonance states [23,39,107]. Furthermore, these two resonance states have different couplings to the meson-baryon states, and $\Lambda(1405)$ state which is dominantly couples to the $\bar{K}N$ state is located at 1420 MeV, instead of the its nominal value 1405 MeV. The other state couples to $\pi\Sigma$ channel which appears around 1390 MeV. This difference may be an important phenomena for the $\bar{K}N$ system, since the position of the $\Lambda(1405)$ resonance is measured from the $\bar{K}N$ threshold. The advent of next-to-leading order (NLO) chiral SU(3) dynamics has enabled the confirmation of the existence of two states, designated as $\Lambda(1405)$ state and $\Lambda(1380)$ state, within the specified energy range [25,52,108,109]. This conclusion has been validated by both the next-to-next-to-leading order (NNLO) analysis [35] and the meson-baryon scattering calculation on the lattice [32,33]. Our mass predictions for K^-p, K^0n, K^-p-K^0n states are located around 1420 MeV (Fig. 2a) and masses of $\pi^+\Sigma^-$, $\pi^-\Sigma^+$, $\pi^0\Sigma^0$, $\pi^+\Sigma^--\pi^-\Sigma^+$, $\pi^+\Sigma^--\pi^0\Sigma^0$ and $\pi^-\Sigma^+-\pi^0\Sigma^0$ states are located around 1330 MeV (Fig. 2b).

3.1.1 Two pole structure of $\Lambda(1405)$

The two-pole structure of the $\Lambda(1405)$ is a prime example of dynamically generated resonances, where the interaction between mesons and baryons leads to the emergence of these states. It is well-established that the $\Lambda(1405)$ exhibits a two-pole structure within the chiral unitary framework, with one pole strongly coupled to the $\bar{K}N$ channel and located closer to 1420 MeV, and the other pole predominantly coupled to the $\pi\Sigma$ channel, appearing around 1390 MeV. This distinction is critical to understanding the resonance nature and the dynamics of the associated channels. The two-pole nature of the $\Lambda(1405)$ was first identified through unitarized chiral perturbation theory, revealing two poles in the complex energy plane, one near the $\bar{K}N$ threshold and the other close to the $\pi\Sigma$ threshold. The higher-mass pole is predominantly a $\bar{K}N$ molecular state, while the lower-mass pole is mainly a composite state of $\pi\Sigma$ with a minor $\bar{K}N$ component [110,111]. The two-pole structure of the $\Lambda(1405)$ is a prime example of dynamically generated resonances, where the interaction between mesons and baryons leads to the emergence of these states. This phenomenon is distinct from other resonances, such as the $N(1440)$ [4], which also exhibit multiple poles but reflect a single state with different characteristics.

Our approach does not explicitly incorporate a coupled-channel formalism capable of resolving the two poles. The OBE model focuses on the meson-baryon molecular configuration and treats the $\bar{K}N$, $\pi\Sigma$, and $\eta\Lambda$ states as independent configurations. While this approach does not explicitly resolve the two-pole structure, it provides insights into the dominant $\bar{K}N$ molecular nature of the higher pole and estimates the spatial sizes and magnetic moments of the associated states. Future extensions of our model could incorporate a coupled-channel analysis to explicitly account for the interplay between the $\bar{K}N$ and $\pi\Sigma$ components and their respective contributions to the two poles.

We focus on exploring the $\Lambda(1405)$ within the meson-baryon molecular configuration using the OBE model, which provides a detailed representation of the meson-baryon interaction potential. Our model treats the $\bar{K}N$, $\pi\Sigma$, and $\eta\Lambda$ states as independent configurations. While it does not explicitly incorporate coupled-channel effects or resolve the two poles, the predicted masses and binding energies in our model align with the higher pole, which is dominantly $\bar{K}N$ like. This supports the interpretation of the $\Lambda(1405)$ as a molecular state in the $\bar{K}N$ channel. This alignment suggests that our results predominantly describe the higher pole of the $\Lambda(1405)$, which is consistent with a dominant $\bar{K}N$ molecular configuration.

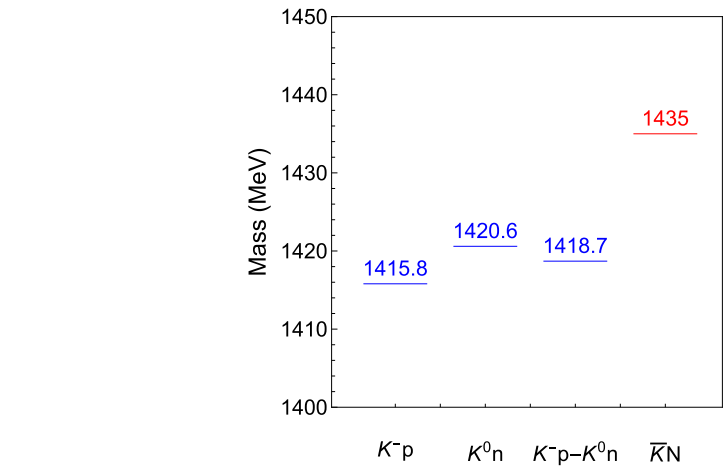

(a) $\bar{K}N$ states

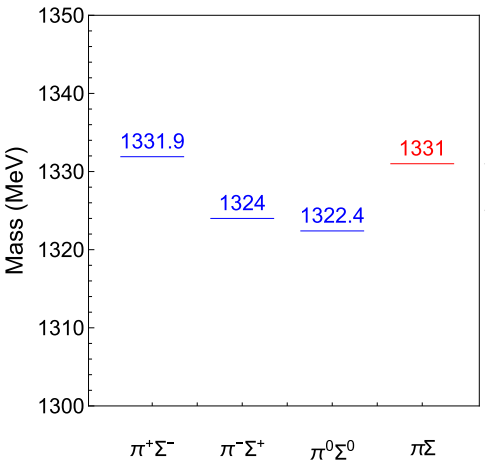

(b) $\pi\Sigma$ states

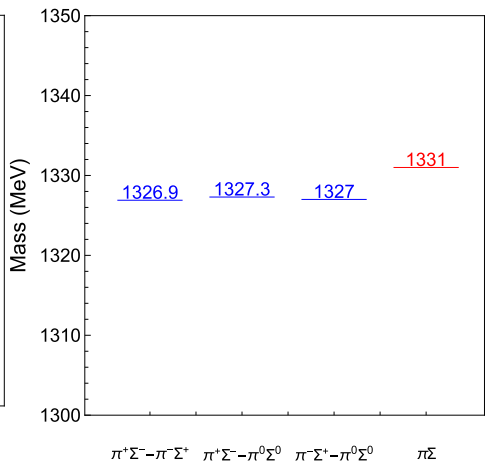

(c) $\pi\Sigma$ states

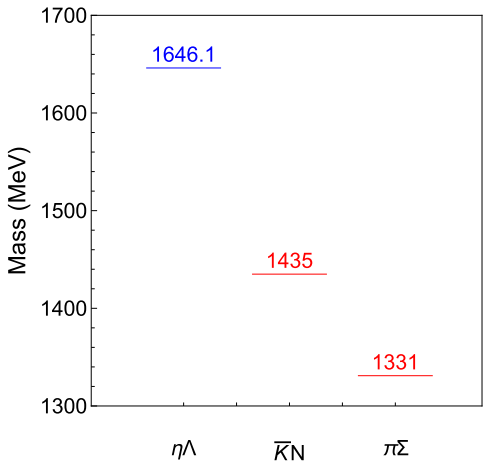

(d) $\eta\Lambda$ state

Fig. 2 Mass locations of $\bar{K}N$, $\pi\Sigma$, and $\pi\Lambda$ states with respect to corresponding thresholds. Blue color refers to calculated masses whereas red color refers to the value of threshold

3.2 Compositeness of the $\bar{K}N$, $\pi\Sigma$, and $\eta\Lambda$ states

We analyze compositeness criterion with respect to Eq. (14). To this end, we first compute the spatial size R values of $\bar{K}N$, $\pi\Sigma$, and $\eta\Lambda$ states. This will also help us to determine the molecular picture of the states under consideration. The information about the size of the hadrons is an important probe for the production yield in the heavy ion collisions estimated by the coalescence model [112]. They found that loosely bound extended molecules with larger size would be formed more abundantly. We present the results in Table 5. As can be seen in the table, K^-p, K^0n, $K^-p - K^0n$, $\pi^+\Sigma^-$, $\pi^-\Sigma^+$, $\pi^0\Sigma^0$, $\pi^+\Sigma^- - \pi^-\Sigma^+$, $\pi^+\Sigma^- - \pi^0\Sigma^0$ and $\pi^-\Sigma^+ - \pi^0\Sigma^0$ and $\eta\Lambda$ states are spatially extended objects. If the $\Lambda(1405)$ state is dominated by the meson-baryon configuration, then it may have a spatially larger size. In Ref. [113], spatial distance of $\bar{K}N$ was evaluated as 1.7 − 1.9 fm. Our results of K^-p, K^0n, and $K^-p - K^0n$ states agree well with this prediction. The obtained size R is bigger than the so-called confinement scale, $(1/\Lambda_{\rm QCD} \sim 1$ fm), supporting the molecular nature of the states of this work.

As mentioned before, in order to distinguish between elementary and composite particles, the field renormalization constant Z is a useful quantity, which gives the probability of finding the elementary component in the physical state, whereas $1 - Z$ gives the measure of compositeness of the state. It was shown in the Weinberg's milestone work that field renormalization constant Z of a weakly bound state can be related to the threshold parameters: the scattering length a_s and the effective range r_e.

The universal properties are one reason why few-body systems with a large scattering length a_s have attracted a lot of attention recently. The low binding energy of the constituents in the hadron implies that scattering length a_s is large. The low-energy universality asserts that the related hadron in molecular picture has properties that depend on a_s but are insensitive to other details of the interactions between the components [114]. In Ref. [115], according to the low-energy universality, it is pointed out for the $X(3872)$ particle that the low-energy few-body observables for nonrelativistic particles with short-range interactions and a large scattering length a_s have universal properties that are insensitive to the details of the mechanism which generates the large scattering length a_s. Therefore if $a_s > 0$, a shallow two-body bound state emerges. On the other side, a shallow S-wave bound state leads a large scattering length a_s compared to the typical length scale of the interaction which implies that the probability for the molecular picture of the related hadron increases as scattering length a_s increases. Weinberg showed that in an elementary state, the value of scattering length a_s would be less than the size of the state R, whilst effective range r_e would be large and negative. As a result, for any composite system r_e should be positive and small rather than negative and large.

Elementariness and compositeness can be decomposed by defining the following relations:

$$\begin{aligned}
&a_s = 0,\ r_e = -\infty \implies \text{purely elementary limit},\ Z = 1,\\
&a_s = R,\ r_e = 0 \implies \text{purely composite limit},\ Z = 0,\\
&a_s \sim R_{\rm typ} \ll -r_e \implies \text{elementary dominance},\ Z \sim 1,\\
&a_s \sim R \gg r_e \sim R_{\rm typ} \implies \text{composite dominance},\ Z \sim 0.
\end{aligned} \tag{28}$$

It should be mentioned that for the criterion in Eq. (28) to be used or say valid, we should remember the weak-binding assumption: the binding energy should be sufficiently small. The typical energy scale is given by

$$E_{\rm typ} = \frac{k_{\rm typ}^2}{2\mu}, \tag{29}$$

where $k_{\rm typ}$ is the typical (smallest) momentum scale of the hadron-hadron interaction and μ is the reduced mass of hadron-hadron system. For the $\bar{K}N$ system, Eq. (29) reads as

$$E_{\rm typ} = \frac{k_{\rm typ}^2}{2\mu} \sim \frac{m_\pi^2}{\mu_{\bar{K}N}} \sim 20\ \text{MeV}. \tag{30}$$

The binding energies of K^-p and K^0n states are found to be as $E_B = 15.9$ MeV and $E_B = 16.6$ MeV, respectively. These binding energies are small than the typical energy scale of the $\bar{K}N$ interaction. Typical energy scales and binding energies for $\pi\Sigma$ and $\eta\Lambda$ states are

$$\begin{aligned}
&E_{\rm typ} \sim 18\ \text{MeV},\ E_B \sim 5\ \text{MeV for}\ \pi\Sigma,\\
&E_{\rm typ} \sim 25\ \text{MeV},\ E_B \sim 17\ \text{MeV for}\ \eta\Lambda.
\end{aligned} \tag{31}$$

In Table 6, scattering length a_s and effective range r_e of the $\bar{K}N$, $\pi\Sigma$, and $\eta\Lambda$ states are presented. These are calculated by using Eq. (14) for different values of field renormalization constant Z. Binding energies are borrowed from Table 4. The range correction $\mathcal{O}(R_{\rm typ})$ is considered as m_ρ. In Figs. 3, 4 and 5 changes in the scattering length a_s, effective range r_e, size of the hadron R and the typical length scale of the interaction $R_{\rm typ}$ with respect to field strength renormalization constant Z for $\bar{K}N$, $\pi\Sigma$, and $\eta\Lambda$ states can be seen, respectively.

In the preceding subsection, the predicted masses of the K^-p, K^0n, and $K^-p - K^0n$ states were determined to be below the threshold of the K^N state. This finding indicates that these states are potential candidates for bound states. As can be seen in Fig. 3, the effective range r_e turns out to be negative when $Z \gtrsim 0.1$ for K^-p and K^0n states whilst it is positive when $Z < 0.1$. For the $K^-p - K^0n$ state, the effective range r_e turns out to be negative when $Z \gtrsim$

Table 5 Spatial size R values of the $\bar{K}N$, $\pi\Sigma$, and $\eta\Lambda$ states. The results are in unit of fm

States	K^-p	K^0n	K^-p-K^0n	$\pi^+\Sigma^-$	$\pi^-\Sigma^+$	$\pi^0\Sigma^0$	$\pi^+\Sigma^- - \pi^-\Sigma^+$	$\pi^+\Sigma^- - \pi^0\Sigma^0$	$\pi^-\Sigma^+ - \pi^0\Sigma^0$	$\eta\Lambda$
R	1.946	1.899	1.918	5.536	5.650	5.575	6.176	6.608	6.252	1.746

Table 6 The scattering length a_s and effective range r_e of $\bar{K}N$, $\pi\Sigma$, and $\eta\Lambda$ states. The values of a_s and r_e are in unit of fm

State	$Z=0$		$Z=0.2$		$Z=0.4$		$Z=0.5$		$Z=0.6$		$Z=0.8$		$Z=1$	
	a_s	r_e	a_s	r_e	a_s	r_e	a_s	r_e	a_s	r_e	a_s	r_e	a_s	r_e
K^-p	2.21	0.26	1.99	− 0.23	1.72	− 1.04	1.56	− 1.69	1.37	− 2.66	0.91	− 7.52	0.26	–
K^0n	2.16	0.26	1.94	− 0.21	1.68	− 1.01	1.53	− 1.64	1.34	− 2.59	0.89	− 7.34	0.26	–
K^-p-K^0n	2.17	0.26	1.96	− 0.22	1.70	− 1.02	1.54	− 1.66	1.35	− 2.62	0.90	− 7.41	0.26	–
$\pi^+\Sigma^-$	5.79	0.26	5.18	− 1.12	4.41	− 3.43	3.95	− 5.28	3.42	− 8.04	2.10	− 21.89	0.26	–
$\pi^-\Sigma^+$	5.91	0.26	5.28	− 1.15	4.50	− 3.51	4.03	− 5.39	3.49	− 8.21	2.14	− 22.34	0.26	–
$\pi^0\Sigma^0$	5.83	0.26	5.21	− 1.13	4.44	− 3.46	3.98	− 5.31	3.44	− 8.10	2.12	− 22.04	0.26	–
$\pi^+\Sigma^- - \pi^-\Sigma^+$	6.43	0.26	5.75	− 1.28	4.89	− 3.86	4.37	− 5.91	3.79	− 9.00	2.32	− 24.44	0.26	–
$\pi^+\Sigma^- - \pi^0\Sigma^0$	6.87	0.26	6.13	− 1.39	5.21	− 4.14	4.66	− 6.34	4.03	− 9.65	2.46	− 26.17	0.26	–
$\pi^-\Sigma^+ - \pi^0\Sigma^0$	6.51	0.26	5.82	− 1.30	4.95	− 3.91	4.43	− 5.99	3.83	− 9.12	2.34	− 24.75	0.26	–
$\eta\Lambda$	2.00	0.26	1.81	− 0.18	1.57	− 0.90	1.42	− 1.49	1.26	− 2.36	0.84	− 6.72	0.26	–

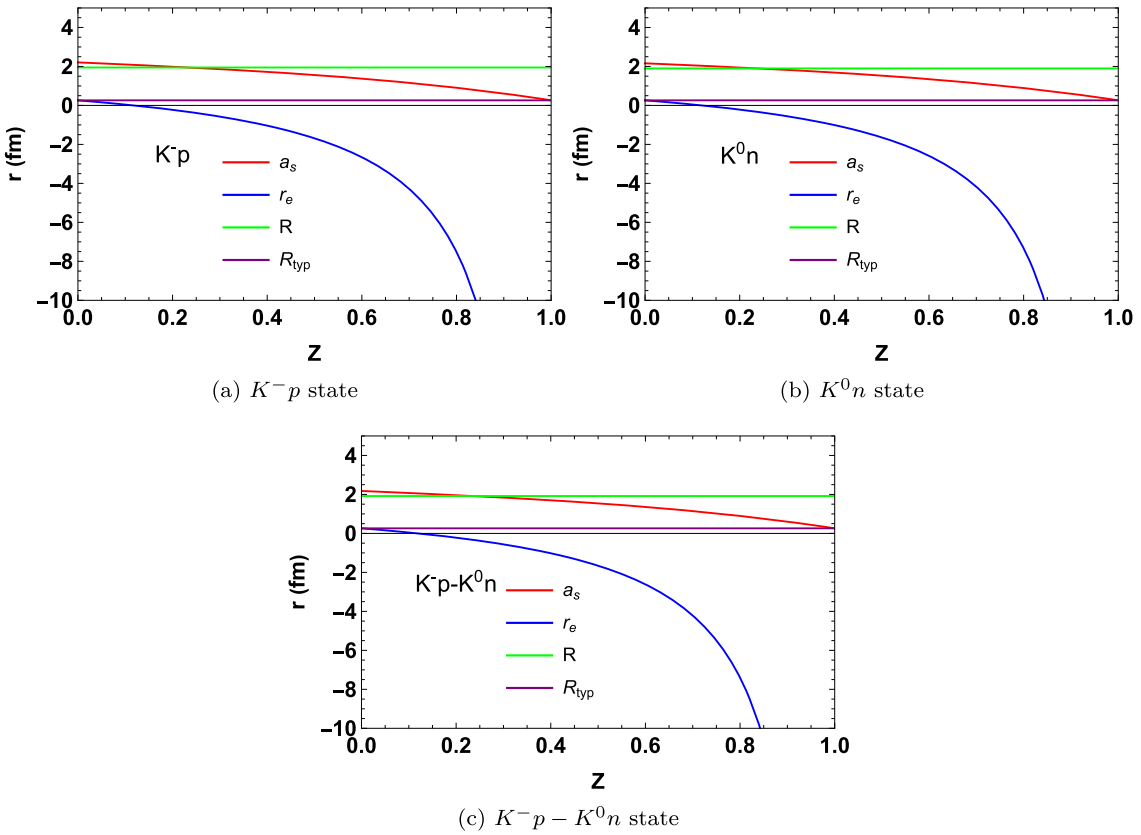

(a) K^-p state (b) K^0n state

(c) K^-p-K^0n state

Fig. 3 Variations of scattering length a_s, effective range r_e, size of the state R, and length scale of interaction R_{typ} with respect changes in field strength renormalization constant Z of $\bar{K}N$ states

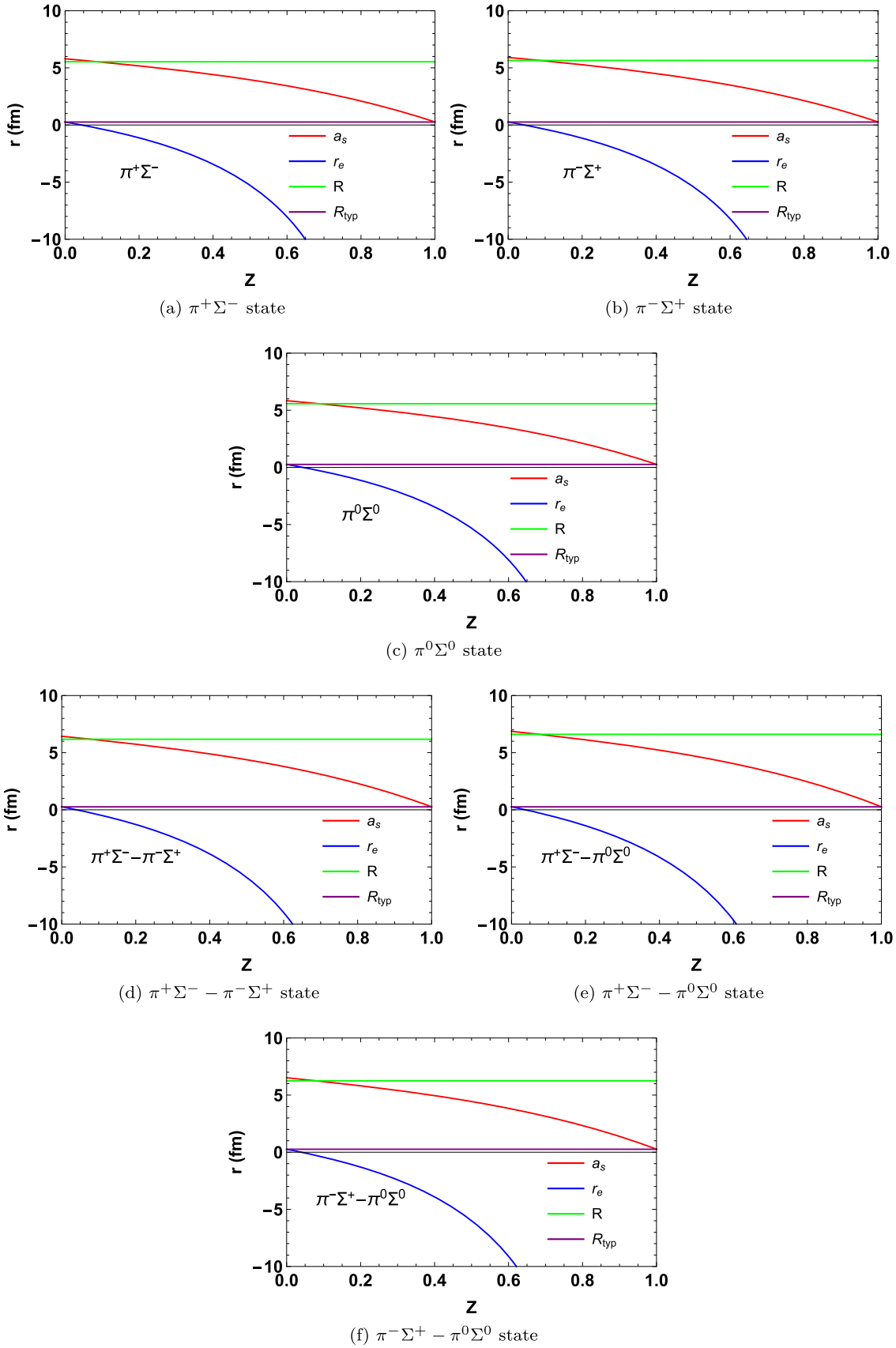

(a) $\pi^+\Sigma^-$ state (b) $\pi^-\Sigma^+$ state

(c) $\pi^0\Sigma^0$ state

(d) $\pi^+\Sigma^- - \pi^-\Sigma^+$ state (e) $\pi^+\Sigma^- - \pi^0\Sigma^0$ state

(f) $\pi^-\Sigma^+ - \pi^0\Sigma^0$ state

Fig. 4 Same as Fig. 3 but for $\pi\,\Sigma$ states

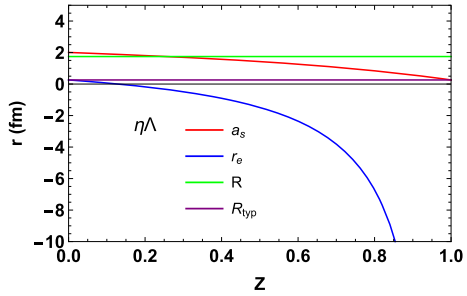

Fig. 5 Same as Fig. 3 but for $\eta\Lambda$ state

0.1 whilst it is positive when $Z < 0.1$. For K^-p, K^0n, and $K^-p - K^0n$ states, a_s is compatible with the size R, $a_s \sim R$ and the value of Z is very close 0. This may be an indicator of the compositeness of these states, namely K^-p, K^0n, and $K^-p - K^0n$ might be molecular states. This conclusion is in line with the Refs. [52,108,109] which obtained compositeness $Z \lesssim 0.1$ for $\Lambda(1405)$ as $\bar{K}N$ state.

The predicted masses of $\pi^+\Sigma^-, \pi^-\Sigma^+, \pi^0\Sigma^0, \pi^+\Sigma^- - \pi^-\Sigma^+, \pi^+\Sigma^- - \pi^0\Sigma^0$ and $\pi^-\Sigma^+ - \pi^0\Sigma^0$ states are found to be lower than the $\pi\Sigma$ threshold. As depicted in Fig. 4, effective range r_e turns out to be positive when $Z \lesssim 0.1$ for $\pi^+\Sigma^-$, $\pi^-\Sigma^+$, $\pi^0\Sigma^0$, $\pi^+\Sigma^- - \pi^-\Sigma^+$, $\pi^+\Sigma^- - \pi^0\Sigma^0$ and $\pi^-\Sigma^+ - \pi^0\Sigma^0$ states. Field strength renormalization constant Z is close to 0. In addition, since $a_s \sim R \gg r_e \sim R_{\text{typ}}$ is satisfied for $\pi^+\Sigma^-, \pi^-\Sigma^+, \pi^0\Sigma^0, \pi^+\Sigma^- - \pi^-\Sigma^+, \pi^+\Sigma^- - \pi^0\Sigma^0$ and $\pi^-\Sigma^+ - \pi^0\Sigma^0$ states, these states might be molecular states.

As is clear in Fig. 2, the mass location of $\eta\Lambda$ state is significantly above thresholds of $\bar{K}N$ and $\pi\Sigma$. This state could be a resonance with respect to corresponding thresholds. Effective range r_e turns out to be positive when $Z < 1$ (Fig. 5).

3.3 Magnetic moments of the $\bar{K}N$, $\pi\Sigma$, and $\eta\Lambda$ states

The study of magnetic moments of the conventional and nonconventional hadrons provides valuable insights into the inner structures and in accordance with this, into the nonperturbative aspects of QCD.

The spatial size of a hadron is a basic quantity which characterizes the structure of a hadron, although it is not directly related to the internal structure. A molecular hadron should have a larger size than the single-hadron whose size is estimated by the energy scale of confinement, ($1/\Lambda_{\text{QCD}} \sim$ 1 fm). In Table 5, the spatial sizes of the $\bar{K}N$, $\pi\Sigma$, and $\eta\Lambda$ states are presented. As is clear from the table, the sizes of the $\bar{K}N$, $\pi\Sigma$, and $\eta\Lambda$ states are larger than the confinement scale. Therefore the subhadrons are distinct objects and it is natural to consider the total magnetic moment as a sum of meson magnetic moment and baryon magnetic moment. The obtained magnetic moments are listed in Table 7. We observe that the magnetic moment of the K^-p, K^0n, $K^-p - K^0n$, $\pi^+\Sigma^-$, $\pi^-\Sigma^+$, $\pi^0\Sigma^0$, $\pi^+\Sigma^- - \pi^-\Sigma^+$, $\pi^+\Sigma^- - \pi^0\Sigma^0$, $\pi^-\Sigma^+ - \pi^0\Sigma^0$, and $\eta\Lambda$ states are composed mainly by the baryons. A similar conclusion was done in Ref. [49] in the $\bar{K}N$ dynamics. The order of the magnetic moments indicates that they are accessible in experimental measurements. A measurement of the magnetic moment of the $\Lambda(1405)$ state may provide an indication for elucidating the inner structure of this state.

We also compare our predictions with the available results. In Ref. [107], magnetic moments of $\Lambda(1405)$ state were calculated by unitarized chiral perturbation theory. In the $\bar{K}N \to \gamma\bar{K}N$, magnetic moment of $\Lambda(1405)$ was obtained as $\mu = 0.44 \pm 0.06\mu_N$ while in the $\bar{K}N \to \gamma\pi\Sigma$ channel, it was obtained as $\mu = 0.26 \pm 0.07$. Our magnetic moment result of $K^-p - K^0n$ agree well with the result of $\bar{K}N \to \gamma\bar{K}N$ channel. In Ref. [61], $\Lambda(1405)$ state was studied in lattice QCD which supported antikaon-nucleon molecule formation. The magnetic moment of $\Lambda(1405)$ state was obtained as $\mu_N = 0.58\mu_N$. In Ref. [76], a futher study was conducted on electromagnetic properties of $\Lambda(1405)$ state by lattice QCD formalism. The magnetic moment was found to be as $\mu_N = 0.63\mu_N$. Our moment result of $K^-p - K^0n$ agree well with these predictions, supporting the $\bar{K}N$ molecular structure of $\Lambda(1405)$ state. Our magnetic moment predictions together with the results in the literature are schematized in Fig. 6. As can be seen in the figure, our prediction of magnetic moment for $\Lambda(1405)$ as $\bar{K}N$ molecular state agree well with the given results in the literature whom support $\bar{K}N$ molecular configuration.

The papers mentioned here adopted molecular nature for the $\Lambda(1405)$ state. In addition to this, the magnetic moment of $\Lambda(1405)$ state was calculated in Ref. [107] using two different sets of parameters. In the $SU(6)$ quark model, $\Lambda(1405)$ can be described as P-wave excitation which give the magnetic moments as $\mu = -0.13\mu_N$ and $\mu = -0.15\mu_N$, for two different sets of parameters. Our results of $\bar{K}N$ states are significantly different than those of conventional picture. However, it is worth to mention that our result of the $\pi^+\Sigma^- - \pi^0\Sigma^0$ state $\mu = -0.117\mu_N$ agree with these results.

4 Final remarks

More than 50 years passed from the observation of $\Lambda(1405)$ state and still it is an intriguing state with properties different from those expected by the quark model. Due to the interesting properties, such as mass and distortion of the line shape from a Breit–Wigner form, this state is still a hot topic in high energy physics. It may be attributed as an old boy of multiquark states.

In this paper, we have studied $\Lambda(1405)$ state considering OBE model and predicted masses, compositeness and

Table 7 Magnetic moments of the $\bar{K}N$, $\pi\Sigma$, and $\eta\Lambda$ states. The results are in unit of nuclear magneton μ_N

States	K^-p	K^0n	K^-p-K^0n	$\pi^+\Sigma^-$	$\pi^-\Sigma^+$	$\pi^0\Sigma^0$	$\pi^+\Sigma^- - \pi^-\Sigma^+$	$\pi^+\Sigma^- - \pi^0\Sigma^0$	$\pi^-\Sigma^+ - \pi^0\Sigma^0$	$\eta\Lambda$
Magnetic moment	2.792	− 1.861	0.465	− 1.047	2.674	0.813	0.814	− 0.117	1.744	− 0.579

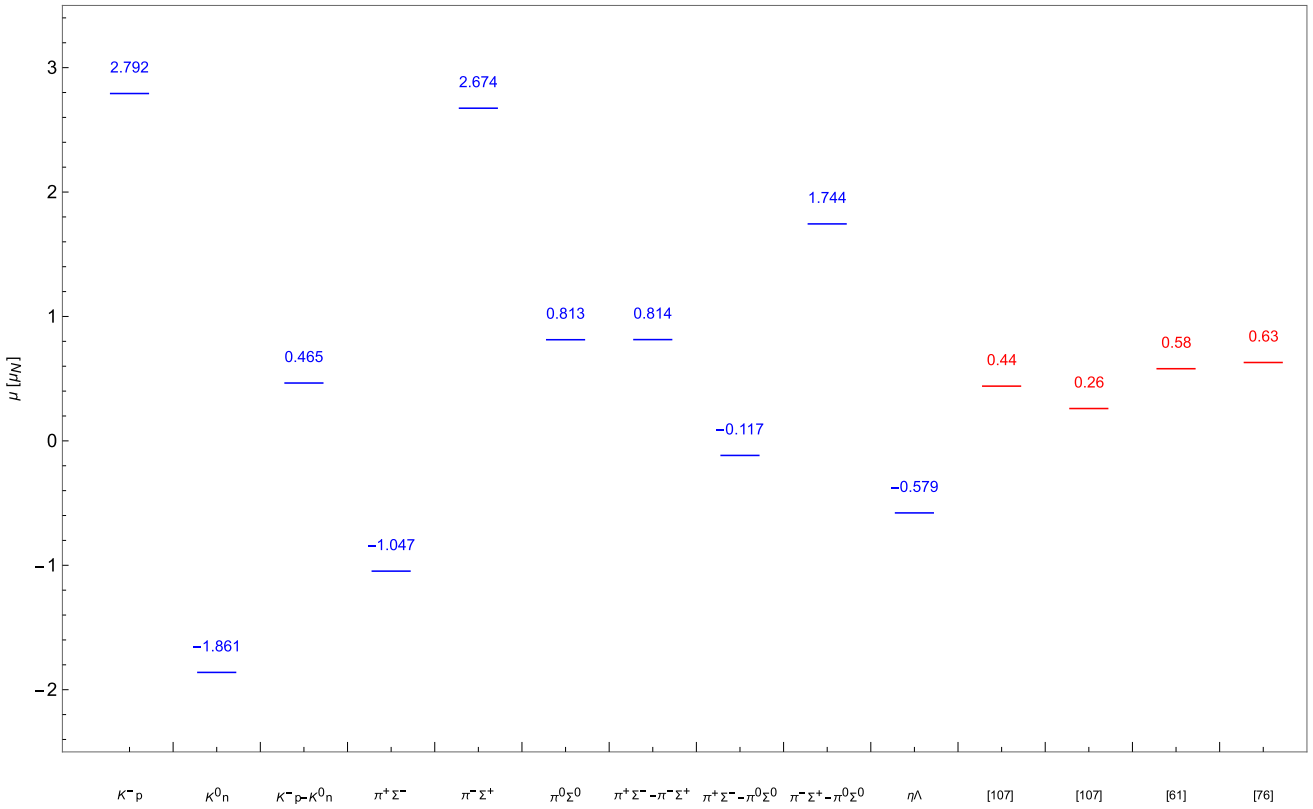

Fig. 6 Comparison of our magnetic moment predictions with those in the literature. Our results are in blue color whereas red colors are from literature

magnetic moments of $\bar{K}N$, $\pi\Sigma$, and $\eta\Lambda$ states which may resemble $\Lambda(1405)$ state at quark level. We assume a meson-baryon molecular configuration for the $\Lambda(1405)$ state. The exploration of meson-baryon molecules provides valuable insights into the nature of strong interactions and the formation of exotic hadronic states. Theoretical predictions and experimental findings continue to advance our understanding of these complex systems, paving the way for future discoveries in the field of hadronic physics. OBE potentials significantly impact nucleon-nucleon scattering observables by providing a framework that incorporates meson exchanges, symmetry considerations, and effective coupling constants. These models can fit experimental data well, especially when accounting for nucleon correlations and renormalization conditions. We highlight our results as follows:

- The mass spectrum of various candidate states, including their binding energies relative to the corresponding thresholds are analyzed.
- The predicted masses of $\bar{K}N$ and $\pi\Sigma$ states are below related thresholds. The binding energies are at the order of 15 MeV for $\bar{K}N$ states and 5 MeV for $\pi\Sigma$ states. These states are bound state candidates with respect to related thresholds. Masses of $\bar{K}N$ states are consistent with the experimental data. The predicted mass of $\eta\Lambda$ state is significantly higher than $\bar{K}N$ and $\pi\Sigma$ thresholds. This state might be a resonance.
- We provide detailed mass predictions that align with the higher-pole structure of the $\Lambda(1405)$ observed in coupled-channel analyses, offering additional evidence for the dominance.
- The coupled-channel analysis of $\Lambda(1405)$ generates a two-pole configuration. The first pole appears around 1420 MeV and called higher pole and the second pole appears around 1390 MeV which is called lower pole. It should be noted that, the pole position is not a direct observable. The mass values of the $\bar{K}N$ states have been

determined to be approximately 1420 MeV, while those of the $\pi\Sigma$ states have been found to be around 1320 MeV.

- We demonstrate that the spatial size of the KN, $\pi\Sigma$, and $\eta\Lambda$ and related states is significantly larger than the confinement scale, supporting their molecular interpretations. The spatial size R values of the $\bar{K}N$, $\pi\Sigma$, and $\eta\Lambda$ states are larger than the energy scale of confinement, $(1/\Lambda_{\rm QCD} \sim 1$ fm). The definition of a hadronic molecule gives sizes larger than 1 fm. The spatial sizes of these states are systematically compared to the confinement scale. Looking the spatial sizes of $\bar{K}N$, $\pi\Sigma$, and $\eta\Lambda$ states, which are at the order of 1.9 fm, 5 fm, and 1.7 fm, respectively; it can be said that these states are hadronic molecules.
- The Weinberg compositeness criterion states that for any composite system effective range r_e should be positive and small rather than negative and large. In addition to this, the field strength renormalization constant Z should be around $Z \sim 0$ for the composite dominance. Effective range r_e of the $\bar{K}N$ states turns out to be small and positive when $Z \lesssim 0.1$. In the case of $\pi\Sigma$ states, the turning point is around $Z \lesssim 0.1$ and for $\eta\Lambda$ state $Z \lesssim 0.1$. Looking Table 6, one can see that the scattering length a_s values for $Z < 0.2$ agree well with the R values presented in Table 5. Furthermore, the compositeness criterion $a_s \sim R \gg r_e \sim R_{\rm typ}$ given in Eq. (28) is fulfilled for all states. This justifies the use of the weak-binding relation to study the compositeness of these states. In addition, the magnitude of the spatial range of the states of this work is larger than the estimated interaction range $R_{\rm typ}$. In Ref. [113], compositeness elaboration of $\Lambda(1405)$ and $\Lambda(1380)$ states was conducted in the the leading order Weinberg-Tomozawa chiral models. The results indicate that the $\bar{K}N$ component is the dominant one in $\Lambda(1405)$. In the case of $\Lambda(1380)$, the largest meson-baryon component is $\pi\Sigma$, although the elemantarity also plays a significant role.
- The compositeness criterion, employing the Weinberg framework to quantitatively assess the molecular nature of the states. The compositeness analysis reveals that these states have a dominant molecular component, with field renormalization constant Z, in agreement with experimental observations and chiral SU(3) dynamics.
- The study of meson-baryon scattering lengths and effective ranges is crucial for understanding the low-energy interactions in hadronic physics. These parameters provide insights into the nature of the forces between mesons and baryons, which are fundamental constituents of matter. The research on meson-baryon scattering lengths and effective ranges encompasses a range of theoretical approaches, including lattice QCD, potential models, and chiral perturbation theory. These studies collectively enhance our understanding of low-energy hadronic interactions, providing valuable parameters that describe the nature of meson-baryon forces.
- The magnetic moments are calculated within the meson-baryon molecular picture using the constituent quark model. These predictions provide valuable informations for future experimental validation. Electromagnetic properties are experimentally testable predictions that can be measured in future studies, offering a direct means of validating the molecular nature of the state.
- The exploration of magnetic moments in exotic hadrons not only enhances our understanding of their internal structures but also aids in the development of more accurate theoretical models. The spatial sizes of the $\bar{K}N$, $\pi\Sigma$, and $\eta\Lambda$ states make enable to use the ansatz for the magnetic moment: magnetic moment of meson-baryon molecule is the sum of the meson magnetic moment and the baryon magnetic moment. Using this ansatz, we have computed the magnetic moments. The order of the magnetic moments are accessible in the experiments. The magnetic moment results scatter between $(-1.8) - (+2.7)$ μ_N. Comparing our results with the available ones in the literature, our result of the $K^-p - K^0n$ molecular state is compatible with the magnetic moment results of the studies which support $\bar{K}N$ molecule configuration. It should be mentioned that, the mesons are in the meson-baryon configurations are pseudoscalar mesons. Therefore they have zero magnetic moments and do not contribute to the total magnetic moment in meson-baryon molecular state. The total magnetic moment of meson-baryon configuration of this model stems from the domination of baryon magnetic moment in the meson-baryon configuration.
- These magnetic moments, along with other electromagnetic properties, are essential for decoding the inner structure of pentaquarks. Experimental measurements of these properties will be crucial in validating theoretical models and enhancing our understanding of the strong interaction in QCD. These studies suggest that the magnetic moments of pentaquark molecular states are crucial for understanding their internal structure and distinguishing between different theoretical models.
- Considering the mass values obtained, it can be seen that masses of K^-p, K^0n, $K^-p - K^0n$, $\pi^+\Sigma^-$, $\pi^-\Sigma^+$, $\pi^0\Sigma^0$, $\pi^+\Sigma^- - \pi^-\Sigma^+$, $\pi^+\Sigma^- - \pi^0\Sigma^0$, $\pi^-\Sigma^+ - \pi^0\Sigma^0$ are below $\bar{K}N$ and $\pi\Sigma$ thresholds except $\eta\Lambda$ state. We observe that all the states of this present work fulfill compositeness criterion. Taking into account the magnetic moment values, magnetic moment of $K^-p - K^0n$ state agree well with the magnetic moments of the molecular $\bar{K}N$ assignment of $\Lambda(1405)$ state.

We hope that the present analysis on $\Lambda(1405)$ mass, spatial size, scattering length and effective range give a good

guideline for forthcoming experiments and lattice QCD calculations. The acquisition of additional experimental data will be instrumental in further elucidating these properties and refining our understanding of hadronic physics.

Data Availability Statement This manuscript has no associated data. [Author's comment: This is a theoretical work. Data sharing not applicable to this article as no datasets were generated or analysed during the current study.]

Code Availability Statement This manuscript has no associated code/software. [Author's comment: This is a theoretical work. Code/Software sharing not applicable to this article as no code/software was generated or analysed during the current study.]

Funded by SCOAP[3].

References

1. R.H. Dalitz, S.F. Tuan, A possible resonant state in pion-hyperon scattering. Phys. Rev. Lett. **2**, 425 (1959). https://doi.org/10.1103/PhysRevLett.2.425
2. M.H. Alston, L.W. Alvarez, P. Eberhard, M.L. Good, W. Graziano, H.K. Ticho, S.G. Wojcicki, Study of resonances of the sigma-pi system. Phys. Rev. Lett. **6**, 698 (1961). https://doi.org/10.1103/PhysRevLett.6.698
3. P.L. Bastien, M. Ferro-Luzzi, A.H. Rosenfeld, Sigma decay modes of pion hyperon resonances. Phys. Rev. Lett. **6**, 702 (1961). https://doi.org/10.1103/PhysRevLett.6.702
4. S. Navas et al. (Particle Data Group), Review of particle physics. Phys. Rev. D **110**, 030001 (2024). https://doi.org/10.1103/PhysRevD.110.030001
5. N. Isgur, G. Karl, P wave baryons in the quark model. Phys. Rev. D **18**, 4187 (1978). https://doi.org/10.1103/PhysRevD.18.4187
6. S. Capstick, N. Isgur, Baryons in a relativized quark model with chromodynamics. Phys. Rev. D **34**, 2809 (1986). https://doi.org/10.1103/physrevd.34.2809
7. Y. Nemoto, N. Nakajima, H. Matsufuru, H. Suganuma, Negative parity baryons in quenched anisotropic lattice QCD. Phys. Rev. D **68**, 094505 (2003). https://doi.org/10.1103/PhysRevD.68.094505. arXiv:hep-lat/0302013
8. T. Hyodo, D. Jido, L. Roca, Structure of the (1405) baryon resonance from its large N(c) behavior. Phys. Rev. D **77**, 056010 (2008). https://doi.org/10.1103/PhysRevD.77.056010. arXiv:0712.3347 [hep-ph]
9. L. Roca, T. Hyodo, D. Jido, On the nature of the Lambda(1405) and Lambda(1670) from their N(c) behavior in chiral dynamics. Nucl. Phys. A **809**, 65 (2008). https://doi.org/10.1016/j.nuclphysa.2008.05.014. arXiv:0804.1210 [hep-ph]
10. E. Oset, A. Ramos, Nonperturbative chiral approach to s wave anti-K N interactions. Nucl. Phys. A **635**, 99 (1998). https://doi.org/10.1016/S0375-9474(98)00170-5. arXiv:nucl-th/9711022
11. Y. Akaishi, T. Yamazaki, Nuclear anti-K bound states in light nuclei. Phys. Rev. C **65**, 044005 (2002). https://doi.org/10.1103/PhysRevC.65.044005
12. D. Strottman, Multi-quark baryons and the MIT bag model. Phys. Rev. D **20**, 748 (1979). https://doi.org/10.1103/PhysRevD.20.748
13. T. Hyodo, D. Jido, A. Hosaka, Origin of the resonances in the chiral unitary approach. Phys. Rev. C **78**, 025203 (2008). https://doi.org/10.1103/PhysRevC.78.025203. arXiv:0803.2550 [nucl-th]
14. T. Sekihara, T. Hyodo, D. Jido, Electromagnetic mean squared radii of Lambda(1405) in chiral dynamics. Phys. Lett. B **669**, 133 (2008). https://doi.org/10.1016/j.physletb.2008.09.023. arXiv:0803.4068 [nucl-th]
15. Y. Akaishi, T. Yamazaki, M. Obu, M. Wada, Single-pole nature of Lambda (1405) and structure of K-pp. Nucl. Phys. A **835**, 67 (2010). https://doi.org/10.1016/j.nuclphysa.2010.01.176. arXiv:1002.2560 [nucl-th]
16. C. Nakamoto, H. Nemura, Lambda(1405) in a hybrid quark model. AIP Conf. Proc. **842**, 458 (2006). https://doi.org/10.1063/1.2220299
17. K. Xu, A. Kaewsnod, Z. Zhao, T.Y. Htun, A. Limphirat, Y. Yan, A possible interpretation of Λ baryon spectrum with pentaquark components. J. Phys. G **50**, 085002 (2023). https://doi.org/10.1088/1361-6471/acd2f2. arXiv:2203.04871 [hep-ph]
18. A. Zhang, Y.R. Liu, P.Z. Huang, W.Z. Deng, X.L. Chen, S.-L. Zhu, J**P = 1/2-pentaquarks in Jaffe and Wilczek's diquark model. HEPNP **29**, 250 (2005). arXiv:hep-ph/0403210
19. N. Kaiser, P.B. Siegel, W. Weise, Chiral dynamics and the low-energy kaon–nucleon interaction. Nucl. Phys. A **594**, 325 (1995). https://doi.org/10.1016/0375-9474(95)00362-5. arXiv:nucl-th/9505043
20. N. Kaiser, T. Waas, W. Weise, SU(3) chiral dynamics with coupled channels: Eta and kaon photoproduction. Nucl. Phys. A **612**, 297 (1997). https://doi.org/10.1016/S0375-9474(96)00321-1. arXiv:hep-ph/9607459
21. I. Zychor et al., Shape of the Lambda(1405) hyperon measured through its sigma0 pi0 decay. Phys. Lett. B **660**, 167 (2008). https://doi.org/10.1016/j.physletb.2008.01.002. arXiv:0705.1039 [nucl-ex]
22. K. Moriya et al. (CLAS), Measurement of the $\Sigma\pi$ photoproduction line shapes near the $\Lambda(1405$. Phys. Rev. C **87**, 035206 (2013). https://doi.org/10.1103/PhysRevC.87.035206. arXiv:1301.5000 [nucl-ex]
23. J.A. Oller, U.G. Meissner, Chiral dynamics in the presence of bound states: Kaon nucleon interactions revisited. Phys. Lett. B **500**, 263 (2001). https://doi.org/10.1016/S0370-2693(01)00078-8. arXiv:hep-ph/0011146
24. L. Roca, E. Oset, Isospin 0 and 1 resonances from $\pi\Sigma$ photoproduction data. Phys. Rev. C **88**, 055206 (2013). https://doi.org/10.1103/PhysRevC.88.055206. arXiv:1307.5752 [nucl-th]
25. M. Mai, U.-G. Meißner, Constraints on the chiral unitary $\bar{K}N$ amplitude from $\pi\Sigma K^+$ photoproduction data. Eur. Phys. J. A **51**, 30 (2015). https://doi.org/10.1140/epja/i2015-15030-3. arXiv:1411.7884 [hep-ph]
26. G. Scheluchin et al. (BGOOD), Photoproduction of K+Λ(1405)→ K+π0Σ0 extending to forward angles and low momentum transfer. Phys. Lett. B **833**, 137375 (2022). https://doi.org/10.1016/j.physletb.2022.137375. arXiv:2108.12235 [nucl-ex]
27. S. Acharya et al. (ALICE), Constraining the $\overline{\mathrm{K}}$N coupled channel dynamics using femtoscopic correlations at the LHC. Eur. Phys. J. C **83**, 340 (2023). https://doi.org/10.1140/epjc/s10052-023-11476-0. arXiv:2205.15176 [nucl-ex]

28. N. Wickramaarachchi, R. A. Schumacher, G. Kalicy (GlueX), Decay of the $\Lambda(1405)$ hyperon to $\Sigma 0\pi 0$ measured at GlueX. EPJ Web Conf. **271**, 07005 (2022), https://doi.org/10.1051/epjconf/202227107005. arXiv:2209.06230 [nucl-ex]
29. A.V. Anisovich, A.V. Sarantsev, V.A. Nikonov, V. Burkert, R.A. Schumacher, U. Thoma, E. Klempt, Hyperon III: $K^- p - \pi\Sigma$ coupled-channel dynamics in the $\Lambda(1405)$ mass region. Eur. Phys. J. A **56**, 139 (2020). https://doi.org/10.1140/epja/s10050-020-00142-8
30. S. Aikawa et al. (J-PARC E31), Pole position of $\Lambda(1405)$ measured in d(K−, n)$\pi\Sigma$ reactions. Phys. Lett. B **837**, 137637 (2023). https://doi.org/10.1016/j.physletb.2022.137637. arXiv:2209.08254 [nucl-ex]
31. M. Conde-Correa, T. Aguilar, A. Capelo-Astudillo, A. Duenas-Vidal, J. Segovia, P.G. Ortega, Chiral quark model analysis of the K$^-$N interaction. Phys. Rev. D **110**, 094019 (2024). https://doi.org/10.1103/PhysRevD.110.094019. arXiv:2407.01759 [hep-ph]
32. J. Bulava et al. (Baryon Scattering (BaSc)), Two-pole nature of the $\Lambda(1405)$ resonance from lattice QCD. Phys. Rev. Lett. **132**, 051901 (2024). https://doi.org/10.1103/PhysRevLett.132.051901. arXiv:2307.10413 [hep-lat]
33. J. Bulava et al. (Baryon Scattering (BaSc)), Lattice QCD study of $\pi\Sigma$-K$^-$N scattering and the $\Lambda(1405)$ resonance. Phys. Rev. D **109**, 014511 (2024). https://doi.org/10.1103/PhysRevD.109.014511. arXiv:2307.13471 [hep-lat]
34. F.-K. Guo, Y. Kamiya, M. Mai, U.-G. Meißner, New insights into the nature of the $\Lambda(1380)$ and $\Lambda(1405)$ resonances away from the SU(3) limit. Phys. Lett. B **846**, 138264 (2023). https://doi.org/10.1016/j.physletb.2023.138264. arXiv:2308.07658 [hep-ph]
35. J.-X. Lu, L.-S. Geng, M. Doering, M. Mai, Cross-channel constraints on resonant antikaon-nucleon scattering. Phys. Rev. Lett. **130**, 071902 (2023). https://doi.org/10.1103/PhysRevLett.130.071902. arXiv:2209.02471 [hep-ph]
36. J.P. Liu, Application of QCD sum rules to the resonance Lambda (1405). Z. Phys. C **22**, 171 (1984). https://doi.org/10.1007/BF01572167
37. S. Choe, Lambda (1405) as a multiquark state. Eur. Phys. J. A **3**, 65 (1998). https://doi.org/10.1007/s100500050148. arXiv:nucl-th/9712003
38. T. Hyodo, What we know about the $\Lambda(1405)$. AIP Conf. Proc. **1735**, 020012 (2016). https://doi.org/10.1063/1.4949380. arXiv:1512.04708 [hep-ph]
39. D. Jido, J.A. Oller, E. Oset, A. Ramos, U.G. Meissner, Chiral dynamics of the two Lambda(1405) states. Nucl. Phys. A **725**, 181 (2003). https://doi.org/10.1016/S0375-9474(03)01598-7. arXiv:nucl-th/0303062
40. Y. Kondo, O. Morimatsu, T. Nishikawa, Y. Kanada-En'yo, Positive and negative-parity flavor-octet baryons in coupled QCD sum rules. Phys. Rev. D **75**, 034010 (2007). https://doi.org/10.1103/PhysRevD.75.034010. arXiv:hep-ph/0610029
41. T. Nakamura, J. Sugiyama, T. Nishikawa, M. Oka, N. Ishii, Exotic quark structure of Lambda(1405) in QCD sum rule. Phys. Lett. B **662**, 132 (2008). https://doi.org/10.1016/j.physletb.2008.02.060. arXiv:0805.1816 [hep-ph]
42. D. Jido, E. Oset, T. Sekihara, Kaonic production of Lambda(1405) off deuteron target in chiral dynamics. Eur. Phys. J. A **42**, 257 (2009). https://doi.org/10.1140/epja/i2009-10875-5. arXiv:0904.3410 [nucl-th]
43. L.S. Kisslinger, E.M. Henley, QCD: the Lambda(1405) as a hybrid. Eur. Phys. J. A **47**, 8 (2011). https://doi.org/10.1140/epja/i2011-11008-5. arXiv:0911.1179 [hep-ph]
44. D. Jido, T. Sekihara, Y. Ikeda, T. Hyodo, Y. Kanada-En'yo, E. Oset, The nature of Lambda(1405) hyperon resonance in chiral dynamics. Nucl. Phys. A **835**, 59 (2010). https://doi.org/10.1016/j.nuclphysa.2010.01.175. arXiv:1003.4560 [nucl-th]
45. C.S. An, B. Saghai, S.G. Yuan, J. He, Role of five-quark components in radiative and strong decays of the Lambda(1405) resonance. Phys. Rev. C **81**, 045203 (2010). https://doi.org/10.1103/PhysRevC.81.045203. arXiv:1002.4085 [nucl-th]
46. A. Martinez Torres, D. Jido, $K\Lambda(1405)$ configuration of the $K\bar{K}N$ system. Phys. Rev. C **82**, 038202 (2010). https://doi.org/10.1103/PhysRevC.82.038202. arXiv:1008.0457 [nucl-th]
47. C. An, B. Saghai, Structure of $\Lambda^*(1405)$ and the Λ^*-meson-baryon coupling constants. Int. J. Mod. Phys. A **26**, 619 (2011). https://doi.org/10.1142/S0217751X11052220. arXiv:1008.1177 [nucl-th]
48. T.T. Takahashi, M. Oka, $\Lambda(1405)$ from lattice QCD. Prog. Theor. Phys. Suppl. **186**, 172 (2010). https://doi.org/10.1143/PTPS.186.172. arXiv:1009.1790 [hep-lat]
49. T. Sekihara, T. Hyodo, D. Jido, Internal structure of resonant Lambda(1405) state in chiral dynamics. Phys. Rev. C **83**, 055202 (2011). https://doi.org/10.1103/PhysRevC.83.055202. arXiv:1012.3232 [nucl-th]
50. B.J. Menadue, W. Kamleh, D.B. Leinweber, M.S. Mahbub, Isolating the $\Lambda(1405)$ in lattice QCD. Phys. Rev. Lett. **108**, 112001 (2012). https://doi.org/10.1103/PhysRevLett.108.112001. arXiv:1109.6716 [hep-lat]
51. A. MartinezTorres, M. Bayar, D. Jido, E. Oset, Strategy to find the two $\Lambda(1405)$ states from lattice QCD simulations. Phys. Rev. C **86**, 055201 (2012). https://doi.org/10.1103/PhysRevC.86.055201. arXiv:1202.4297 [hep-lat]
52. Z.-H. Guo, J.A. Oller, Meson-baryon reactions with strangeness −1 within a chiral framework. Phys. Rev. C **87**, 035202 (2013). https://doi.org/10.1103/PhysRevC.87.035202. arXiv:1210.3485 [hep-ph]
53. M. Mai, U.-G. Meissner, New insights into antikaon-nucleon scattering and the structure of the Lambda(1405). Nucl. Phys. A **900**, 51 (2013). https://doi.org/10.1016/j.nuclphysa.2013.01.032. arXiv:1202.2030 [nucl-th]
54. J. Revai, Signature of the $\Lambda(1405)$ resonance in neutron spectra from the $K^- + d$ reaction. Few Body Syst. **54**, 1865 (2013). https://doi.org/10.1007/s00601-013-0694-1. arXiv:1203.1813 [nucl-th]. [Erratum: Few Body Syst. 54, 1877 (2013)]
55. T. Sekihara, S. Kumano, Determination of compositeness of the $\Lambda(1405)$ resonance from its radiative decay. Phys. Rev. C **89**, 025202 (2014). https://doi.org/10.1103/PhysRevC.89.025202. arXiv:1311.4637 [nucl-th]
56. J.A. Oller, New insights in $\bar{K}N$ scattering and the $\Lambda(1405)$. Int. J. Mod. Phys. Conf. Ser. **26**, 1460096 (2014). https://doi.org/10.1142/S2010194514600969. arXiv:1309.2196 [nucl-th]
57. S.X. Nakamura, D. Jido, Lambda (1405) photoproduction based on chiral unitary model. PTEP **2014**, 023D01 (2014). https://doi.org/10.1093/ptep/ptt121. arXiv:1310.5768 [nucl-th]
58. S.X. Nakamura, D. Jido, Theoretical analysis of $\Lambda(1405)$ photoproduction. PoS Hadron **Hadron2013**, 141 (2013). https://doi.org/10.22323/1.205.0141. arXiv:1312.6768 [nucl-th]
59. B.J. Menadue, W. Kamleh, D.B. Leinweber, M. Selim Mahbub, B.J. Owen, Electromagnetic form factors for the $\Lambda(1405)$. PoS **LATTICE2013**, 280 (2014). https://doi.org/10.22323/1.187.0280. arXiv:1311.5026 [hep-lat]
60. T. Sekihara, S. Kumano, Determining compositeness of hadronic resonances: the $\Lambda(1405)$ radiative decay and the $a_0(980)$-$f_0(980)$ mixing. JPS Conf. Proc. **8**, 022006 (2015). https://doi.org/10.7566/JPSCP.8.022006. arXiv:1411.3414 [hep-ph]
61. J.M.M. Hall, W. Kamleh, D.B. Leinweber, B.J. Menadue, B.J. Owen, A.W. Thomas, R.D. Young, Lattice QCD evidence that the $\Lambda(1405)$ resonance is an antikaon-nucleon molecule. Phys. Rev. Lett. **114**, 132002 (2015). https://doi.org/10.1103/PhysRevLett.114.132002. arXiv:1411.3402 [hep-lat]
62. A. Doté, T. Myo, Double-pole nature of $\Lambda(1405)$ studied with coupled-channel complex scaling method using complex-range

Gaussian basis. Nucl. Phys. A **930**, 86 (2014). https://doi.org/10.1016/j.nuclphysa.2014.08.041. arXiv:1406.1540 [nucl-th]
63. S. Ohnishi, Y. Ikeda, T. Hyodo, E. Hiyama, W. Weise, $K^- d \to \pi \Sigma n$ reactions and structure of the $\Lambda(1405)$. J. Phys. Conf. Ser. **569**, 012077 (2014). https://doi.org/10.1088/1742-6596/569/1/012077. arXiv:1408.0118 [nucl-th]
64. S. Ohnishi, Y. Ikeda, T. Hyodo, W. Weise, Structure of the $\Lambda(1405)$ and the $K^- d \to \pi \Sigma n$ reaction. Phys. Rev. C **93**, 025207 (2016). https://doi.org/10.1103/PhysRevC.93.025207. arXiv:1512.00123 [nucl-th]
65. S.-i. Nam, H.-K. Jo, Photoproduction of $\Lambda(1405)$ with the two-pole structure. (2015). arXiv:1503.00419 [hep-ph]
66. J.M.M. Hall, W. Kamleh, D.B. Leinweber, B.J. Menadue, B.J. Owen, A.W. Thomas, R.D. Young, On the structure of the Lambda 1405. PoS **LATTICE2014**, 094 (2014). https://doi.org/10.22323/1.214.0094
67. K. Miyahara, T. Hyodo, Structure of $\Lambda(1405)$ and construction of $\overline{K}N$ local potential based on chiral SU(3) dynamics. Phys. Rev. C **93**, 015201 (2016). https://doi.org/10.1103/PhysRevC.93.015201. arXiv:1506.05724 [nucl-th]
68. K. Miyahara, T. Hyodo, E. Oset, Weak decay of Λ_c^+ for the study of $\Lambda(1405)$ and $\Lambda(1670)$. Phys. Rev. C **92**, 055204 (2015). https://doi.org/10.1103/PhysRevC.92.055204. arXiv:1508.04882 [nucl-th]
69. K. Miyahara, T. Hyodo, Construction of $\overline{K}$N potential and structure of $\Lambda(1405)$ based on chiral unitary approach. JPS Conf. Proc. **10**, 022011 (2016). https://doi.org/10.7566/JPSCP.10.022011. arXiv:1508.07707 [nucl-th]
70. K. Miyahara, T. Hyodo, Composite nature of $\Lambda(1405)$ from the spacial structure of $\bar{K}N$ system. JPS Conf. Proc. **17**, 073001 (2017). https://doi.org/10.7566/JPSCP.17.073001. arXiv:1512.02735 [nucl-th]
71. J. He, P.-L. Lu, The octet meson and octet baryon interaction with strangeness and the $\Lambda(1405)$. Int. J. Mod. Phys. E **24**, 1550088 (2015). https://doi.org/10.1142/S0218301315500883. arXiv:1510.00580 [nucl-th]
72. C. Fernandez-Ramirez, I.V. Danilkin, V. Mathieu, A.P. Szczepaniak, Understanding the nature of $\Lambda(1405)$ through Regge physics. Phys. Rev. D **93**, 074015 (2016). https://doi.org/10.1103/PhysRevD.93.074015. arXiv:1512.03136 [hep-ph]
73. R. Molina, M. Döring, Pole structure of the $\Lambda(1405)$ in a recent QCD simulation. Phys. Rev. D **94**, 056010 (2016). https://doi.org/10.1103/PhysRevD.94.079901. arXiv:1512.05831 [hep-lat]. [Addendum: Phys. Rev. D 94, 079901 (2016)]
74. Y. Kamiya, K. Miyahara, S. Ohnishi, Y. Ikeda, T. Hyodo, E. Oset, W. Weise, Antikaon-nucleon interaction and $\Lambda(1405)$ in chiral SU(3) dynamics. Nucl. Phys. A **954**, 41 (2016). https://doi.org/10.1016/j.nuclphysa.2016.04.013. arXiv:1602.08852 [hep-ph]
75. Z.-W. Liu, J.M.M. Hall, D.B. Leinweber, A.W. Thomas, J.-J. Wu, Structure of the **$\Lambda(1405)$** from Hamiltonian effective field theory. Phys. Rev. D **95**, 014506 (2017). https://doi.org/10.1103/PhysRevD.95.014506. arXiv:1607.05856 [nucl-th]
76. J.M.M. Hall, W. Kamleh, D.B. Leinweber, B.J. Menadue, B.J. Owen, A.W. Thomas, Light-quark contributions to the magnetic form factor of the Lambda(1405). Phys. Rev. D **95**, 054510 (2017). https://doi.org/10.1103/PhysRevD.95.054510. arXiv:1612.07477 [hep-lat]
77. F.-Y. Dong, B.-X. Sun, J.-L. Pang, The $\Lambda(1405)$ state in a chiral unitary approach with off-shell corrections to dimensional regularized loop functions. Chin. Phys. C **41**, 074108 (2017). https://doi.org/10.1088/1674-1137/41/7/074108. arXiv:1609.08354 [nucl-th]
78. S.-H. Kim, S.-I. Nam, D. Jido, H.-C. Kim, Photoproduction of $\Lambda(1405)$ with the N^* and t-channel Regge contributions. Phys. Rev. D **96**, 014003 (2017). https://doi.org/10.1103/PhysRevD.96.014003. arXiv:1702.08645 [hep-ph]
79. J.Y. Süngü, N. Er, Nuclear medium effects on the properties of $\Lambda(1405)$. J. Phys. G **51**, 125001 (2024). https://doi.org/10.1088/1361-6471/ad66eb. arXiv:2403.02728 [nucl-th]
80. H. Yukawa, On the interaction of elementary particles I. Proc. Phys. Math. Soc. Jpn. **17**, 48 (1935). https://doi.org/10.1143/PTPS.1.1
81. M. Taketani, S. Machida, S. O-numa, The meson theory of nuclear forces, I*: the deuteron ground state and low energy neutron-proton scattering. Prog. Theor. Phys. **7**, 45 (1952). https://doi.org/10.1143/ptp/7.1.45 https://academic.oup.com/ptp/article-pdf/7/1/45/5428018/7-1-45.pdf
82. S. Sawada, T. Ueda, W. Watari, M. Yonezawa, One boson exchange model in proton-proton scattering*: an approach to the strong interaction. Prog. Theor. Phys. **28**, 991 (1962). https://doi.org/10.1143/PTP.28.991 https://academic.oup.com/ptp/article-pdf/28/6/991/5202298/28-6-991.pdf
83. G. Breit, Nucleon-nucleon spin-orbit interaction and the repulsive core. Phys. Rev. **120**, 287 (1960). https://doi.org/10.1103/PhysRev.120.287
84. M. Karliner, J.L. Rosner, Exotic resonances due to η exchange. Nucl. Phys. A **954**, 365 (2016). https://doi.org/10.1016/j.nuclphysa.2016.03.057. arXiv:1601.00565 [hep-ph]
85. M. SanchezSanchez, L.-S. Geng, J.-X. Lu, T. Hyodo, M.P. Valderrama, Exotic doubly charmed $D_{s0}^*(2317)D$ and $D_{s1}^*(2460)D^*$ molecules. Phys. Rev. D **98**, 054001 (2018). https://doi.org/10.1103/PhysRevD.98.054001. arXiv:1707.03802 [hep-ph]
86. T. Sekihara, Y. Kamiya, T. Hyodo, $N\Omega$ interaction: meson exchanges, inelastic channels, and quasibound state. Phys. Rev. C **98**, 015205 (2018). https://doi.org/10.1103/PhysRevC.98.015205. arXiv:1805.04024 [hep-ph]
87. M.-Z. Liu, T.-W. Wu, M. Sánchez Sánchez, M.P. Valderrama, L.-S. Geng, J.-J. Xie, Spin-parities of the $P_c(4440)$ and $P_c(4457)$ in the one-boson-exchange model. Phys. Rev. D **103**, 054004 (2021). https://doi.org/10.1103/PhysRevD.103.054004. arXiv:1907.06093 [hep-ph]
88. F.-L. Wang, X.-D. Yang, R. Chen, X. Liu, Hidden-charm pentaquarks with triple strangeness due to the $\Omega_c^{(*)}\bar{D}_s^{(*)}$ interactions. Phys. Rev. D **103**, 054025 (2021). https://doi.org/10.1103/PhysRevD.103.054025. arXiv:2101.11200 [hep-ph]
89. F. Gross, A. Stadler, High-precision covariant one-boson-exchange potentials for np scattering below 350-MeV. Phys. Lett. B **657**, 176 (2007). https://doi.org/10.1016/j.physletb.2007.10.028. arXiv:0704.1229 [nucl-th]
90. F. Gross, D.O. Riska, Current conservation and interaction currents in relativistic meson theories. Phys. Rev. C **36**, 1928 (1987). https://doi.org/10.1103/PhysRevC.36.1928
91. A. Stadler, F. Gross, Relativistic calculation of the triton binding energy and its implications. Phys. Rev. Lett. **78**, 26 (1997). https://doi.org/10.1103/PhysRevLett.78.26. arXiv:nucl-th/9607012
92. A. Stadler, F. Gross, M. Frank, Covariant equations for the three-body bound state. Phys. Rev. C **56**, 2396 (1997). https://doi.org/10.1103/PhysRevC.56.2396. arXiv:nucl-th/9703043
93. F.-K. Guo, C. Hanhart, U.-G. Meißner, Q. Wang, Q. Zhao, B.-S. Zou, Hadronic molecules. Rev. Mod. Phys. **90**, 015004 (2018). https://doi.org/10.1103/RevModPhys.90.015004. arXiv:1705.00141 [hep-ph]. [Erratum: Rev. Mod. Phys. 94, 029901 (2022)]
94. R. Machleidt, K. Holinde, C. Elster, The Bonn meson exchange model for the nucleon nucleon interaction. Phys. Rep. **149**, 1 (1987). https://doi.org/10.1016/S0370-1573(87)80002-9
95. R. Machleidt, The High precision, charge dependent Bonn nucleon-nucleon potential (CD-Bonn). Phys. Rev. C **63**, 024001 (2001). https://doi.org/10.1103/PhysRevC.63.024001. arXiv:nucl-th/0006014

96. A.M. Badalian, A.I. Veselov, B.L.G. Bakker, Restriction on the strong coupling constant in the IR region from the 1D–1P splitting in bottomonium. Phys. Rev. D **70**, 016007 (2004). https://doi.org/10.1103/PhysRevD.70.016007
97. D. Ebert, R.N. Faustov, V.O. Galkin, Mass spectra and Regge trajectories of light mesons in the relativistic quark model. Phys. Rev. D **79**, 114029 (2009). https://doi.org/10.1103/PhysRevD.79.114029. arXiv:0903.5183 [hep-ph]
98. M. Naghdi, Nucleon-nucleon interaction: a typical/concise review. Phys. Part. Nucl. **45**, 924 (2014). https://doi.org/10.1134/S1063779614050050. arXiv:nucl-th/0702078
99. S. Weinberg, Elementary particle theory of composite particles. Phys. Rev. **130**, 776 (1963). https://doi.org/10.1103/PhysRev.130.776
100. S. Weinberg, Evidence that the deuteron is not an elementary particle. Phys. Rev. **137**, B672 (1965). https://doi.org/10.1103/PhysRev.137.B672
101. S. Klarsfeld, J. Martorell, D.W.L. Sprung, Deuteron properties and the nucleon nucleon interaction. J. Phys. G **10**, 165 (1984). https://doi.org/10.1088/0305-4616/10/2/008
102. C. Van Der Leun, C. Alderliesten, The deuteron binding energy. Nucl. Phys. A **380**, 261 (1982). https://doi.org/10.1016/0375-9474(82)90105-1
103. G.-J. Wang, R. Chen, L. Ma, X. Liu, S.-L. Zhu, Magnetic moments of the hidden-charm pentaquark states. Phys. Rev. D **94**, 094018 (2016). https://doi.org/10.1103/PhysRevD.94.094018. arXiv:1605.01337 [hep-ph]
104. F. Guo, H.-S. Li, Analysis of the hidden-charm pentaquark states based on magnetic moment and transition magnetic moment. Eur. Phys. J. C **84**, 392 (2024). https://doi.org/10.1140/epjc/s10052-024-12699-5. arXiv:2304.10981 [hep-ph]
105. H.-S. Li, F. Guo, Y.-D. Lei, F. Gao, Magnetic moments and axial charges of the octet hidden-charm molecular pentaquark family. Phys. Rev. D **109**, 094027 (2024). https://doi.org/10.1103/PhysRevD.109.094027. arXiv:2401.14767 [hep-ph]
106. G.-J. Wang, L. Meng, H.-S. Li, Z.-W. Liu, S.-L. Zhu, Magnetic moments of the spin-$\frac{1}{2}$ singly charmed baryons in chiral perturbation theory. Phys. Rev. D **98**, 054026 (2018). https://doi.org/10.1103/PhysRevD.98.054026. arXiv:1803.00229 [hep-ph]
107. D. Jido, A. Hosaka, J.C. Nacher, E. Oset, A. Ramos, Magnetic moments of the Lambda(1405) and Lambda(1670) resonances. Phys. Rev. C **66**, 025203 (2002). https://doi.org/10.1103/PhysRevC.66.025203. arXiv:hep-ph/0203248
108. Y. Ikeda, T. Hyodo, W. Weise, Improved constraints on chiral SU(3) dynamics from kaonic hydrogen. Phys. Lett. B **706**, 63 (2011). https://doi.org/10.1016/j.physletb.2011.10.068. arXiv:1109.3005 [nucl-th]
109. Y. Ikeda, T. Hyodo, W. Weise, Chiral SU(3) theory of antikaon-nucleon interactions with improved threshold constraints. Nucl. Phys. A **881**, 98 (2012). https://doi.org/10.1016/j.nuclphysa.2012.01.029. arXiv:1201.6549 [nucl-th]
110. K. Miyahara, T. Hyodo, W. Weise, Construction of a local $\bar{K}N-\pi\Sigma-\pi\Lambda$ potential and composition of the $\Lambda(1405)$. Phys. Rev. C **98**, 025201 (2018). https://doi.org/10.1103/PhysRevC.98.025201. arXiv:1804.08269 [nucl-th]
111. Z.-Y. Wang, H.A. Ahmed, C.W. Xiao, Is two-pole's $\Lambda(1405)$ one state or two? Eur. Phys. J. C **81**, 833 (2021). https://doi.org/10.1140/epjc/s10052-021-09633-4. arXiv:2106.10511 [hep-ph]
112. S. Cho et al. (ExHIC), Multi-quark hadrons from heavy ion collisions. Phys. Rev. Lett. **106**, 212001 (2011). https://doi.org/10.1103/PhysRevLett.106.212001. arXiv:1011.0852 [nucl-th]
113. T. Sekihara, T. Hyodo, Size measurement of dynamically generated hadronic resonances with finite boxes. Phys. Rev. C **87**, 045202 (2013). https://doi.org/10.1103/PhysRevC.87.045202. arXiv:1209.0577 [nucl-th]
114. L. Platter, Low-energy universality in atomic and nuclear physics. Few Body Syst. **46**, 139 (2009). https://doi.org/10.1007/s00601-009-0057-0. arXiv:0904.2227 [nucl-th]
115. E. Braaten, M. Kusunoki, Low-energy universality and the new charmonium resonance at 3870-MeV. Phys. Rev. D **69**, 074005 (2004). https://doi.org/10.1103/PhysRevD.69.074005. arXiv:hep-ph/0311147